

Mutations in Three Genes Encoding Proteins Involved in Hair Shaft Formation Cause Uncombable Hair Syndrome

F. Buket Ü. Basmanav,^{1,2,3} Laura Cau,^{4,23} Aylar Tafazzoli,^{1,23} Marie-Claire Méchin,^{4,23} Sabrina Wolf,¹ Maria Teresa Romano,¹ Frederic Valentin,⁵ Henning Wiegmann,⁵ Anne Huchencq,⁴ Rima Kandil,¹ Natalie Garcia Bartels,⁶ Arzu Kilic,⁷ Susannah George,⁸ Damian J. Ralser,¹ Stefan Bergner,¹ David J.P. Ferguson,⁹ Ana-Maria Oprisoreanu,¹⁰ Maria Wehner,¹ Holger Thiele,¹¹ Janine Altmüller,^{11,12} Peter Nürnberg,^{11,13,14} Daniel Swan,¹⁵ Darren Houniet,¹⁵ Aline Büchner,¹⁶ Lisa Weibel,^{16,17} Nicola Wagner,¹⁸ Ramon Grimalt,¹⁹ Anette Bygum,²⁰ Guy Serre,⁴ Ulrike Blume-Peytavi,⁶ Eli Sprecher,²¹ Susanne Schoch,¹⁰ Vinzenz Oji,⁵ Henning Hamm,²² Paul Farrant,⁸ Michel Simon,^{4,23} and Regina C. Betz^{1,23,*}

Uncombable hair syndrome (UHS), also known as “spun glass hair syndrome,” “pili trianguli et canaliculi,” or “cheveux incoiffables” is a rare anomaly of the hair shaft that occurs in children and improves with age. UHS is characterized by dry, frizzy, spangly, and often fair hair that is resistant to being combed flat. Until now, both simplex and familial UHS-affected case subjects with autosomal-dominant as well as -recessive inheritance have been reported. However, none of these case subjects were linked to a molecular genetic cause. Here, we report the identification of UHS-causative mutations located in the three genes *PADI3* (peptidylarginine deiminase 3), *TGM3* (transglutaminase 3), and *TCHH* (trichohyalin) in a total of 11 children. All of these individuals carry homozygous or compound heterozygous mutations in one of these three genes, indicating an autosomal-recessive inheritance pattern in the majority of UHS case subjects. The two enzymes *PADI3* and *TGM3*, responsible for posttranslational protein modifications, and their target structural protein *TCHH* are all involved in hair shaft formation. Elucidation of the molecular outcomes of the disease-causing mutations by cell culture experiments and tridimensional protein models demonstrated clear differences in the structural organization and activity of mutant and wild-type proteins. Scanning electron microscopy observations revealed morphological alterations in hair coat of *Padi3* knockout mice. All together, these findings elucidate the molecular genetic causes of UHS and shed light on its pathophysiology and hair physiology in general.

Introduction

UHS (MIM: 191480), was first described as a distinctive hair shaft defect in 1973.^{1,2} However, the phenotype had been recognized far earlier and had obtained notoriety as the famous literary character “Struwelpeter” (“Shockheaded Peter”) from the children’s story published by the German physician Heinrich Hoffmann in 1845. This was later translated by Mark Twain to English as “Slovenly Peter.” Up to now about 100 UHS cases have been reported.^{3–5} Most of the cases are simplex occurrences but autosomal-dominant or -recessive inheritance patterns were also

observed. In majority of the cases, UHS is an isolated condition of the hair, but it has occasionally been observed with additional symptoms, such as ectodermal dysplasias, retinopathia pigmentosa, juvenile cataract, and polydactyly. Isolated UHS is characterized by silvery, blond, or straw-colored scalp hair that is dry, frizzy, and wiry, has a characteristic sheen, stands away from the scalp in multiple directions, and is impossible to comb. This hair shaft disorder occurs in children and improves with age. The hair growth rate can range from slow to normal. The clinical diagnosis of UHS can be confirmed by scanning electron microscopy (SEM) analysis of hair shafts.^{6–8} In at least

¹Institute of Human Genetics, University of Bonn, 53127 Bonn, Germany; ²Department of Neuro- and Sensory Physiology, University Medical Center Göttingen, 37073 Göttingen, Germany; ³Campus Laboratory for Advanced Imaging, Microscopy and Spectroscopy, University of Göttingen, 37073 Göttingen, Germany; ⁴CNRS UMR5165 and INSERM U1056 and University of Toulouse, 31059 Toulouse, France; ⁵Department of Dermatology, University of Münster, 48149 Münster, Germany; ⁶Clinical Research Center for Hair and Skin Science, Department of Dermatology and Allergy, Charité-Universitätsmedizin Berlin, Berlin 10117, Germany; ⁷Dermatology Department, Balikesir University School of Medicine, 10100 Balikesir, Turkey; ⁸Dermatology Department, Brighton and Sussex University Hospitals NHS Trust, Brighton General Hospital, Elm Grove, Brighton BN2 3EW, UK; ⁹Nuffield Department of Clinical Laboratory Science, University of Oxford, John Radcliffe Hospital, Oxford OX3 9DU, UK; ¹⁰Department of Neuropathology and Department of Epileptology, University of Bonn, 53127 Bonn, Germany; ¹¹Cologne Center for Genomics, University of Cologne, 50931 Cologne, Germany; ¹²Institute of Human Genetics, University of Cologne, 50931 Cologne, Germany; ¹³Center for Molecular Medicine Cologne, University of Cologne, 50931 Cologne, Germany; ¹⁴Cologne Excellence Cluster on Cellular Stress Responses in Aging-Associated Diseases, University of Cologne, 50931 Cologne, Germany; ¹⁵Computational Biology Group, Oxford Gene Technology, Oxford OX5 1PF, UK; ¹⁶Pediatric Dermatology Department, University Children’s Hospital Zurich, University Hospital of Zurich, 8032 Zurich, Switzerland; ¹⁷Dermatology Department, University Hospital Zurich, 8032 Zurich, Switzerland; ¹⁸Clinical Center Darmstadt, 64297 Darmstadt, Germany; ¹⁹Universitat Internacional de Catalunya, Sant Cugat del Vallès, 08195 Barcelona, Spain; ²⁰Department of Dermatology and Allergy Centre, Odense University Hospital, 5000 Odense, Denmark; ²¹Department of Dermatology, Tel Aviv Sourasky Medical Center, Tel Aviv 64239, Israel; ²²Department of Dermatology, Venereology, and Allergology, University Hospital Würzburg, 97080 Würzburg, Germany

²³These authors contributed equally to this work

*Correspondence: regina.betz@uni-bonn.de

<http://dx.doi.org/10.1016/j.ajhg.2016.10.004>

© 2016 American Society of Human Genetics.

50% of the hair examined, this reveals a triangular or heart-shaped cross-section, in comparison to the normal circular cross section, as well as longitudinal grooves along the entire length of the hair shaft.⁹ The hair is not more fragile or brittle than normal hair. No effective therapy is yet available although biotin supplementation was reported to be successful in some cases.¹⁰

Until now, no genetic alteration had been linked to UHS although familial occurrence has been well observed. In this study, we report UHS causative mutations in *PADI3* (MIM: 606755), *TGM3* (MIM: 600238), and *TCHH* (MIM: 190370), encoding for hair shaft proteins that display sequential interactions with each other. Transfection of cells with constructs encoding for wild-type (WT) and mutant proteins showed that the identified *PADI3* and *TGM3* mutations have profound effects on enzymatic activity of the respective proteins. The observation of alterations in whiskers and hair coat of *Padi3* knockout mice confirms the essential role of this enzyme in hair shaft morphology. Altogether, our findings indicate that UHS occurs when interactions of a structural protein that gives shape and mechanical strength to the hair shaft are impaired by defects either in this protein itself or in others that mediate its interactions.

Material and Methods

Study Participants

Detailed information regarding the clinical descriptions of the individuals included in this study is given in the [Supplemental Case Reports](#). This study was performed according to the principles of the Declaration of Helsinki. Ethical approval was obtained from the ethics committee of the Medical Faculty of the University of Bonn and the participants provided written informed consent prior to blood sampling. Written informed consents of the affected individuals or their legal guardians were obtained for the publication of the case photos included in this manuscript.

Scanning Electron Microscopy

Hair shafts from various individuals with UHS and control subjects were mounted on stubs and sputter coated with either gold or platinum prior to examination in either a FEI Quanta FEG250 or a Philips 505 scanning electron microscope.

Exome Sequencing

Exome sequencing was performed in two different centers. The two affected siblings of the discovery family from UK were exome sequenced by Oxford Gene Technology's GeneEfficiency Sequencing Service. Genomic DNA (2 µg) was fragmented and enriched for human exonic sequences using the Human All Exon V5 Agilent Sure Select kit (Agilent Technologies) using the manufacturer's protocol and sequenced on the Illumina HiSeq 2000 platform using Truseq (v3 Chemistry) (Illumina) to generate 100 base paired-end reads. Fastq files were mapped to the reference human genome (hg19/GRCh37) using the Burrows-Wheeler Aligner (BWA) package (v.0.6.2).¹¹ Local realignment of the mapped reads around potential insertion/deletion (indel) sites was carried out with the Genome Analysis Tool Kit (GATK) v.1.6.¹² Duplicate reads

were marked using Picard v.1.8 and BAM files were sorted and indexed with SAM tools v.0.1.18.¹³ Approximately 12 and 14 GB of sequence data was generated for these samples and a minimum of 90.83% and 80.54% of the targeted exome was covered to a depth of at least 20× and 30× coverage, respectively. We filtered the variants for high-quality homozygous or potentially compound heterozygous, novel variants (defined against dbSNP 132 inclusion) that are shared by both siblings and are deleterious based on either of the SIFT, PolyPhen, and Condel predictions.

The affected individuals from Germany and Turkey were exome sequenced at the Cologne Center for Genomics. For whole-exome sequencing, 1 µg of genomic DNA was fragmented with sonication technology (Bioruptor, Diagenode). The fragments were end-repaired and adaptor ligated, including incorporation of sample index barcodes. After size selection, a pool of all five libraries was subjected to an enrichment process with the SeqCap EZ Human Exome Library v.2.0 kit (Roche NimbleGen). The final libraries were sequenced on an Illumina HiSeq 2000 sequencing instrument (Illumina) with a paired-end 2 × 100 bp protocol. Primary data were filtered according to signal purity by the Illumina Real-time Analysis (RTA) software v.1.8. Subsequently, the reads were mapped to the human genome reference build hg19 using the BWA-aln alignment algorithm.¹¹ GATK v.1.6 was used to mark duplicated reads, to do a local realignment around short insertions and deletions, to recalibrate the base quality scores, and to call SNPs and short indels.¹² For the Turkish individual, this resulted in 7.5 Gb of unique mapped sequences, a mean coverage of 94×, and 30× coverage of 91% of the target sequences. For the German individual, this resulted in 8.1 Gb of unique mapped sequences, a mean coverage of 106×, and 30× coverage of 92% of the target sequences. The Varbank pipeline v.2.10 and interface developed in-house at the Cologne Center for Genomics were used for data analysis and filtering (unpublished data, H.T., J.A., and P.N.). The GATK UnifiedGenotyper variation calls were filtered for high-quality (DP > 15; AF > 0.25 + VQSLOD > -8 if possible, otherwise: QD > 2; MQ > 40; FS < 60; MQRankSum > -12.5; ReadPosRankSum > -8; HaplotypeScore < 13) rare (MAF ≤ 0.005 based on 1000 Genomes build 20110521 and EVS build ESP6500) variants, predicted to modify a protein sequence or to impair splicing, in homozygous or compound heterozygous state.

Sanger Sequencing

Amplicons were generated under standard polymerase chain reaction conditions by using primers presented in [Tables S1–S3](#). Sanger sequencing was performed using the BigDye Terminator v.1.1 Cycle Sequencing kit (Applied Biosystems) and an ABI 3100 genetic analyzer (Applied Biosystems). The data were analyzed using SeqMan II software (DNASTAR).

Molecular Cloning and Mammalian Cell Cultures

To construct the expression vectors for *PADI3* and *TGM3*, the coding sequences (cDNA) of *PADI3* (1,995 bp) and *TGM3* (2,082 bp) were amplified from hair follicle cDNA and cloned into the TOPO cloning site of pcDNA 3.1/V5-His-TOPO vector (Invitrogen) according to manufacturer's protocol. The mutant constructs (*PADI3*: c.335T>A [p.Leu112His], c.881C>T [p.Ala294Val], c.1813C>A [p.Pro605Thr]; and *TGM3*: c.1351C>T [p.Gln451*]) were generated by targeted mutagenesis using QuickChange II Site-Directed Mutagenesis kit (Agilent Technologies) according to manufacturer's instructions. The constructs were verified by Sanger sequencing. The primers used for cloning and mutagenesis

are listed in Table S4. The HaCaT human keratinocyte cell line was established by Boukamp et al.¹⁴ The HEK293T cell line was a kind gift from Thomas Zillinger (Institute of Clinical Chemistry and Clinical Pharmacology, University of Bonn). Both HaCaT and HEK293T cell lines were tested for mycoplasma contamination and confirmed to be mycoplasma free. Cells were maintained at 37°C (5% CO₂) in DMEM (Lonza) supplemented with 10% FCS (Life Technologies), 1% penicillin-streptomycin (10,000 U mL⁻¹, Life Technologies), and 1% Amphotericin B (250 µg mL⁻¹, Life Technologies). Cells were cultured in 10 cm Petri dishes and on coverslips in 24-well plates for western blotting and immunofluorescence analysis, respectively. Transfections were carried on using the Lipofectamine3000 Transfection Kit (Life Technologies) according to manufacturer's instructions. For each 10 cm plate, the following amounts of reagents were used: 15 µg plasmid, 1,500 µL Opti-MEM (Life Technologies), 22.5 µL Lipofectamine3000, and 30 µL P3000 reagent. For each well in a 24-well plate, 0.5 µg of plasmid, 50 µL Opti-MEM, 1.5 µL Lipofectamine3000, and 1 µL P3000 reagent were used. Cells were harvested 48 hr after transfection.

Topological Tridimensional Models of PADI3

We constructed, as we had previously published,¹⁵ a topological tridimensional model of WT PADI3 using the crystal atomic coordinates of calcium-bound human PADI4 (MIM: 605347; PDB: 1WDA).¹⁶ On this basis, topological models of the tridimensional structure of the three mutated enzymes were produced after in silico substitutions of the respective amino acids. All the models were refined by energy minimization (3 × 3,000 iterations) using the MSI insight II modules Biopolymer, CHARMM, and Viewer on an O2 SGI station. Energetic potentials after minimization were all improved and validated. The three models were then validated by analyses of "Anolea data" and Ramachandran plots produced using the Swiss model expasy structure assessment tools and the Swiss-Pdb viewer software v.4.04, respectively. Finally, topological models of mutated PADI3 were individually compared to that of WT PADI3 after a magic fit on Swiss-Pdb viewer. Solid ribbon representations were displayed to show overviews of the tridimensional structures or enlargements focused on either the catalytic sites or the five calcium binding sites.

Immunoblotting of HaCaT and HEK293T Cell Extracts

Cells were collected in ice-cold PBS and centrifuged at 150 × *g* at 4°C for 10 min. The cell pellets were re-suspended in 40 µL of 10× RIPA buffer (Cell Signaling Technology) and 360 µL Protease Inhibitor Cocktail (Roche), incubated on ice for 15 min, and sonicated 10 times for 10 s, with 10 s breaks on ice. After centrifugation at 10,500 × *g* for 10 min at 4°C, the supernatants were transferred to clean tubes and purified with Micro Bio-Spin Columns (Bio-Rad Laboratories) according to manufacturer's instructions. Purified lysates were mixed with 4× Laemmli sample buffer (Bio-Rad Laboratories) diluted in β-mercaptoethanol. After protein separation on TGX stain-free gels 4%–15% (Bio-Rad Laboratories), the proteins were transferred on PVDF membrane (Amersham Biosciences). Western blotting was carried out using the WesternBreeze chemiluminescent kit (Invitrogen) according to manufacturer's instructions. The following primary antibodies were used with an incubation duration of 1 hr: mouse monoclonal anti-V5 (1:5,000, Sigma Aldrich cat# V8012; RRID: AB_261888) and rabbit monoclonal anti-PADI3/PAD3 (1:400, Abcam cat# ab172959) for PADI3 detection and mouse monoclonal anti-Flag (1:5,000,

Sigma Aldrich cat# F1804; RRID: AB_262044) and rabbit polyclonal anti TGM3-C-terminal (1:250, Aviva Systems Biology cat# OAAB12971) for TGM3 detection. Membranes were developed using the ChemiDoc MP imager (Bio Rad) for a maximum of 20 min. Data in Figure 4A are representative of western blotting experiments from three independent transfections of HaCaT cells with PADI3 constructs. Data in Figures 7A and S7 emerge from six independent transfections of HaCaT (1×) and HEK293T (5×) cells with TGM3 constructs. The relative quantities of WT and mutated TGM3 were assessed using Stain-Free technology that is based on total protein normalization (Bio-Rad Laboratories).¹⁷

Immunofluorescence Analysis in HaCaT and HEK293T Cells

Transiently transfected HaCaT and HEK293T cells grown on coverslips were washed with 1× PBS for 5 min, permeabilized for 10 min with 1% Triton X-100, and blocked for 1 hr in PBS containing 1% bovine serum albumin, 10% normal goat serum, and 0.1% Triton X-100. The cells were incubated with mouse monoclonal anti-V5 primary antibody (1:100, Sigma Aldrich cat# V8012; RRID: AB_261888) or mouse monoclonal anti-Flag antibody (1:500, Sigma Aldrich cat# F1804; RRID: AB_262044) for PADI3 and TGM3, respectively, for 3 hr at RT (or overnight at 4°C) and goat anti-mouse-cy3 secondary antibody (1:500, Life Technologies cat# A10521; RRID: AB_2534030) with DAPI (Sigma Aldrich cat# D9542) for 40 min. The mounting was performed with Mowiol 4-88 (Roth). Images were captured with 63× or 10× oil immersion objectives using a Zeiss Axioplan 2 imaging microscope and the Cytovision 7.4 software. ImageJ was used for the analyses by applying the same brightness and contrast thresholds to all data. Data presented in Figures 4B and 7B are representative of analyses from four independent transfections of HaCaT cells with PADI3 constructs and five independent transfections of HaCaT (3×) and HEK293T (2×) cells with TGM3 constructs, respectively. Two to three coverslips were analyzed per construct at each transfection.

Activity of PADI3 in HaCaT Cells

Transiently transfected HaCaT cells grown on coverslips were air-dried. For indirect immunofluorescence, the cells were rehydrated for 15 min in PBS and permeabilized for 10 min in PBS containing 1% Triton X-100, and then non-specific binding sites were blocked with PBS containing 2% fetal bovine serum and 1% Triton X-100. Slides were incubated with the following primary antibodies: mouse monoclonal anti-V5 (1:100, Thermo Fisher Scientific cat# R960-25; RRID: AB_2556564) and ACPA antibodies (6 µg mL⁻¹) purified from a pool of sera of individuals affected by rheumatoid arthritis (MIM: 180300).^{18,19} Sera were from informed and consenting individuals attending the Rheumatology Center of Toulouse and have been declared to and approved by the Comité de Protection des Personnes Sud Ouest et Outre-Mer II (Toulouse, France). After incubation with the corresponding secondary antibodies, Alexa Fluor 488 Donkey anti-mouse IgG (1:10,000, Thermo Fisher Scientific cat# A-21202; RRID: AB_2535788), Alexa Fluor 555 Goat Anti-human IgG (H+L) (1:10,000, Thermo Fisher Scientific cat# A21433; RRID: AB_1500626), and DAPI (Sigma-Aldrich cat# D9542), slides were mounted in Mowiol 4-88 (Calbiochem Merck Millipore). Images were captured with 20× dry or 63× oil immersion objectives using a Zeiss apotome microscope (Carl Zeiss). ImageJ was used for the analyses by applying the same brightness and contrast thresholds to all data. Data



Figure 1. Clinical Appearance of UHS

(A–G) Clinical presentation of UHS. Typical signs of UHS can be observed in three German girls (A–C), a German boy (D), a Swiss boy (E), and a Danish girl (F and G), who were included in the study. The improvement of the phenotype with aging can be observed in the Danish girl (G).

(H and I) SEM image of the Danish girl's hair shaft showing the longitudinal groove (H) in comparison to a normal (I) hair shaft.

(J–M) The improved hair phenotype at age 15 (J) and the SEM findings (K and L) of the male sibling from the UK family. Shown are longitudinal grooves (K) and heart-shaped cross section (L) of altered hairs, both indicative of UHS, in comparison to the circular cross section from a control hair shaft (M).

Detailed information regarding the clinical histories can be found in the [Supplemental Case Reports](#).

presented in [Figure 5A](#) are representative of analyses from two independent transfections of HaCaT cells with three coverslips for each single *PADI3* construct.

Activity of PADI3 Produced in *Escherichia coli*

E. coli strain BL21(DE3)-pLysS (Life Technologies) were transformed with 5 ng of the recombinant expression plasmids (pcDNA3.1/V5-His-TOPO-*PADI3*-WT, pcDNA3.1/V5-His-TOPO-*PADI3*-p.Leu112His, pcDNA3.1/V5-His-TOPO-*PADI3*-p.Arg294Val, and pcDNA3.1/V5-His-TOPO-*PADI3*-p.Pro605Thr) and grown at 37°C overnight on agar-Luria Broth plates (MP Biomedicals) supplemented with ampicillin (50 µg mL⁻¹) and chloramphenicol (34 µg mL⁻¹). Four clones were selected for each plasmid. After selection, the bacterial clones were grown in Luria Broth medium supplemented with ampicillin (50 µg mL⁻¹) at 37°C for 3 hr and then overnight at 30°C. Harvested bacteria were sonicated 4 × 8 s (6–10 W) on ice in a Tris-HCl (pH 7.6) buffer containing a cocktail of bacterial protease inhibitors (Sigma Aldrich). After centrifugation at 9,000 × *g* for 10 min, soluble proteins were recovered in the supernatants (clarified extracts).

To measure an in vitro deimination activity, the clarified extracts were incubated at 37°C in 100 mM Tris-HCl (pH 7.6) buffer containing 10 mM CaCl₂ and 5 mM DTT, for either 2 hr or overnight,

under agitation at 1,400 rpm.²⁰ The deimination reactions were stopped by boiling for 3 min in Laemmli's sample buffer. The proteins were then separated by SDS-polyacrylamide (10%) gel electrophoresis and immunodetected with the V5 Epitope Tag monoclonal antibody (1:5,000, Thermo Fisher Scientific cat# R960-25; RRID: AB_2556564) and the anti-modified citrulline antibodies.^{21,22} The blots were developed using the ECL prime system (GE Healthcare) as described by the manufacturer. Immunoblotting signals were recorded using a G:Box Chemi XT4 imager and GeneTool analysis software (Syngene) for a maximum of 20 min.

After one bacteria transformation, two independent clones for p.Leu112His, three for p.Pro605Thr, and four for WT and p.Ala294Val were analyzed, with identical results; only those corresponding to two clones are illustrated. Data are representative of two technical replicates. The V5-antibody detections of recombinant PADI3 were confirmed using an anti-PADI3 antibody.²²

Padi3-Deficient Mice

All experiments with animals were approved by a local ethic committee (INSERM US006 CEEA-122) and carried out according to our institution guidelines and EU legislation. *Padi3*-deficient mice (B6NCrI;B6N-A^{tm1Brd}*Padi3*^{tm1a(KOMP)Wtsi}/Or, abbreviated to *Padi3*^{tm1a}) were generated by the Phenomin Program at the ICS

Table 1. Individuals Carrying *PADI3*, *TGM3*, and *TCHH* Mutations

Country	Gene	Mutation	Consequence	Clinical Description
United Kingdom	<i>PADI3</i>	c.881C>T, homozygous	p.Ala294Val	this study
Denmark	<i>PADI3</i>	c.881C>T, homozygous	p.Ala294Val	Nissen and Svendsen ²⁴
Germany	<i>PADI3</i>	c.335T>A, homozygous	p.Leu112His	this study
Spain	<i>PADI3</i>	c.881C>T, c.335T>A	p.Ala294Val, p.Leu112His	Novoa et al. ²⁵
Germany	<i>PADI3</i>	c.881C>T, c.335T>A	p.Ala294Val, p.Leu112His	this study
Germany	<i>PADI3</i>	c.881C>T, c.335T>A	p.Ala294Val, p.Leu112His	this study
Germany	<i>PADI3</i>	c.881C>T, c.1813C>A	p.Ala294Val, p.Pro605Thr	this study
Germany	<i>PADI3</i>	c.335T>A, c.1813C>A	p.Leu112His, p.Pro605Thr	this study
Switzerland	<i>PADI3</i>	c.881C>T, c.1732A>T	p.Ala294Val, p.Lys578*	this study
Turkey	<i>TGM3</i>	c.1351C>T, homozygous	p.Gln451*	Kilic et al. ²⁶
Germany	<i>TCHH</i>	c.991C>T, homozygous	p.Gln331*	this study

Laboratory (Strasbourg, France). A promoter-less *LacZ*-reporter cassette containing a neomycin-resistance gene and flanked by two flippase recognition target sites was inserted between exons 4 and 5 of *Padi3*, with *loxP* sites flanking the exons 5 and 6. (See International Mouse Phenotyping Consortium website in the [Web Resources](#) for more details.) Mice were maintained in the TAAM animal facility (CNRS UPS44, Orléans, France) under pathogen-free conditions. They were killed by cervical dislocation. All efforts were made to minimize suffering. The following oligonucleotides were used for genotyping: *Padi3* forward (5'-CTTTATTGATAAACACAGGCAGGGAGC-3'), *Padi3* reverse (5'-CAATGGAATCCCTCTGTCCCTCACC-3'), and *LacZ* reverse (5'-CCAACAGCTTCCCCACAACGG-3'). A wild-type PCR product of 241 bp and a *tm1a* allele product of 365 bp were produced. Genotyping was confirmed using the *Padi3* forward (5'-CCC TCTTTGAGGACCACAGGCTTATC-3') and reverse (5'-GCACTCAA GAAGCAGAGGCAGGC-3') primers, a wild-type PCR product of 369 bp, and a *tm1a* allele product of 421 bp were produced. No randomization was used. The SEM observations of whiskers and hair coat were done in blind, by two independent scientists.

Transglutaminase Activity of *TGM3*

In order to compare the enzymatic activity of WT and mutant *TGM3* in cell extracts of transiently transfected HEK293T cells, we adapted the transglutaminase assay described by Aufenvenne et al.²³ This assay is based on the incorporation of monodansylcadaverine into casein by transglutaminase, which causes an augmentation of fluorescence and an emission wavelength shift. Lysates of cells transiently transfected with WT or mutant *TGM3* constructs were prepared 48 hr after transfection as described in the immunoblotting section. Lysates of mock-transfected cells were used as a negative control. The translation of the target proteins was always confirmed by immunoblotting. For the assay, the lysates were incubated for 15 min in pre-warmed assay buffer (50 mM Tris/HCl, 10 mM CaCl₂, 10 mM reduced glutathione, 2.5% glycerol, 2.5% DMSO, 25 μM monodansylcadaverine, 20 mM N,N-dimethylcasein [pH 8]) at 37°C. Measurements were then made for 10 min at 37°C using a LS55 fluorescence spectrometer (Perkin Elmer) with excitation and emission wavelengths of 332 nm and 500 nm, respectively, and a 5.0 nm slit. The linear

slopes of the measurements from technical triplicates of samples emerging from five independent transfections were used as a measure of the transglutaminase activity.²³ The activity data were not normally distributed ($p < 0.050$, Shapiro-Wilk) and analyzed by a Kruskal-Wallis test (one-way ANOVA on Ranks) with post hoc Dunn's pairwise multiple comparisons test.

Results

Identification of Mutations in *PADI3*, *TGM3*, and *TCHH*

In this study, we identified UHS-causative mutations in three functionally related genes in a total of 11 individuals/families (Figure 1, Table 1; Supplemental Case Reports). The first family originated from the UK and had two affected and two unaffected siblings. The affected individuals reported typical hair problems in childhood with improvement when growing older (Figure 1J); gross and scanning electron microscopy observations were in line with an UHS phenotype (Figures 1K and 1L). In order to elucidate the genetic background of UHS in this family, we performed whole-exome sequencing (WES) in both of the affected siblings. We filtered the data for novel and deleterious homozygous or potentially compound heterozygous variants that are shared by the siblings and identified a homozygous missense variant c.881C>T (p.Ala294Val) within *PADI3* (GenBank: NM_016233.2). The mutation co-segregated with the disease phenotype in the family (Figures 2A and S1).

Then, we Sanger sequenced *PADI3* in 17 additional case subjects and detected the above-mentioned mutation as well as two other recurrent missense mutations, c.335T>A (p.Leu112His) and c.1813C>A (p.Pro605Thr), in seven other individuals/families (Table 1, Figures 2B, 2C, and S2).^{24,25} We also identified an individual who carries c.881C>T (p.Ala294Val) and a nonsense mutation, c.1732A>T (p.Lys578*), that occurred only once in

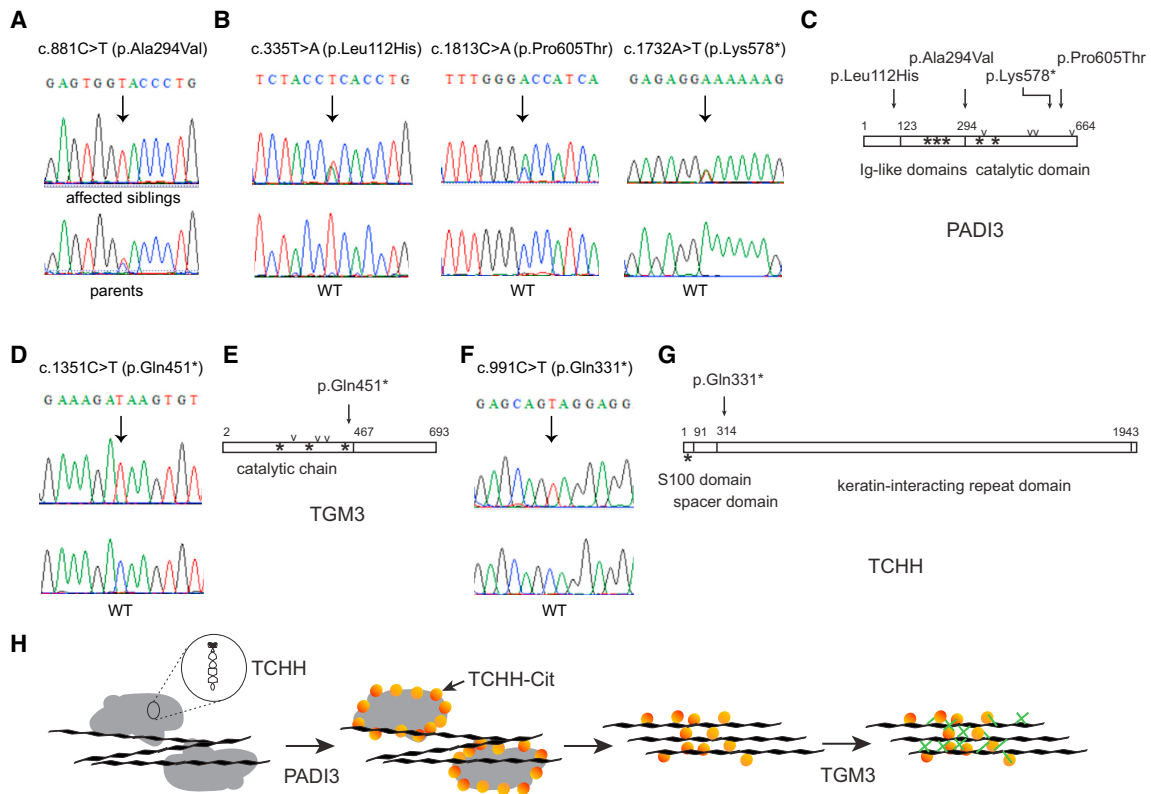


Figure 2. Mutations Causing UHS and Interplay of PADI3, TGM3, and TCHH

(A) The homozygous c.881C>T (p.Ala294Val) mutation in *PADI3* identified by exome sequencing in the UK siblings was verified by Sanger sequencing. The mutation co-segregates with the UHS phenotype in the pedigree as shown in Figure S1.

(B) Electropherograms show the *PADI3* mutations c.335T>A (p.Leu112His), c.1813C>A (p.Pro605Thr), and c.1732A>T (p.Lys578*) in comparison to the wild-type sequences.

(C) Schematic representation of *PADI3* showing the various domains of the protein and the positions of calcium-binding sites (*) and of major amino acids involved in the catalytic sites (v). The positions of the substitutions responsible for UHS are indicated by an arrow.

(D) Electropherograms show the homozygous *TGM3* mutation c.1351C>T (p.Gln451*) identified in the Turkish male in comparison to the wild-type sequence.

(E) Schematic representation of *TGM3*.

(F) Electropherograms show the homozygous *TCHH* mutation c.991C>T (p.Gln331*) identified in the German female in comparison to the wild-type sequence.

(G) Schematic representation of *TCHH*.

(H) Cartoon depicting the cascade of interactions between *TCHH*, *PADI3*, and *TGM3* in hair shaft biology. In trichohyalin granules (gray areas), *TCHH* appears as a dimer with a long rod-shaped domain and a globular end domain. After deimination by *PADI3*, *TCHH* is less structured, and the granules progressively dissolved. Citrullinated-*TCHH* (*TCHH-Cit*) interacts with keratin intermediate filaments (black lines) organizing them, and becomes a substrate for *TGM3*. Cross-links of *TCHH* to itself (intra- or inter-chains), to keratins and between keratins and the cornified cell envelope components are then catalyzed (green dash).

our UHS cohort (Table 1, Figures 2B, 2C, and S2). These mutations were observed either in homozygous state or in compound heterozygosity as confirmed by parental DNA sequencing in three of the families (Figure S1). The allele frequencies of the *PADI3* substitutions from Exome Aggregation Consortium (ExAC) data are presented in Table S5. The nonsense mutation was not observed in ExAC.

As a next step, we performed WES in four further UHS-affected case subjects with no *PADI3* mutations. We identified the nonsense mutation c.1351C>T (p.Gln451*) in *TGM3* (GenBank: NM_003245.3) in a Turkish individual²⁶ and the nonsense mutation c.991C>T (p.Gln331*) in *TCHH* (GenBank: NM_007113.3) in a German individual (Figures 2D–2G; Table S5). No homozygous loss-of-

function mutations were observed in *TGM3* or *TCHH* in ~60,000 sequenced individuals of the ExAC database.

PADI3, TGM3, and TCHH Interplay in Hair Shaft Formation

PADI3, a gene of the *PADI* family (*PADI1-4* and *6*), encodes the 664-amino acid peptidylarginine deiminase type III (Enzyme Commission: EC.3.5.3.15).²⁷ This posttranslational modification enzyme converts positively charged L-arginine residues of proteins into neutral citrulline residues in the presence of calcium ions. The process is called deimination or citrullination. *PADI3* is mainly detected in skin, including hair follicles where it modifies hair shaft proteins.^{28,29} Although the enzyme has already been a focus of interest in hair biology, it could not be linked

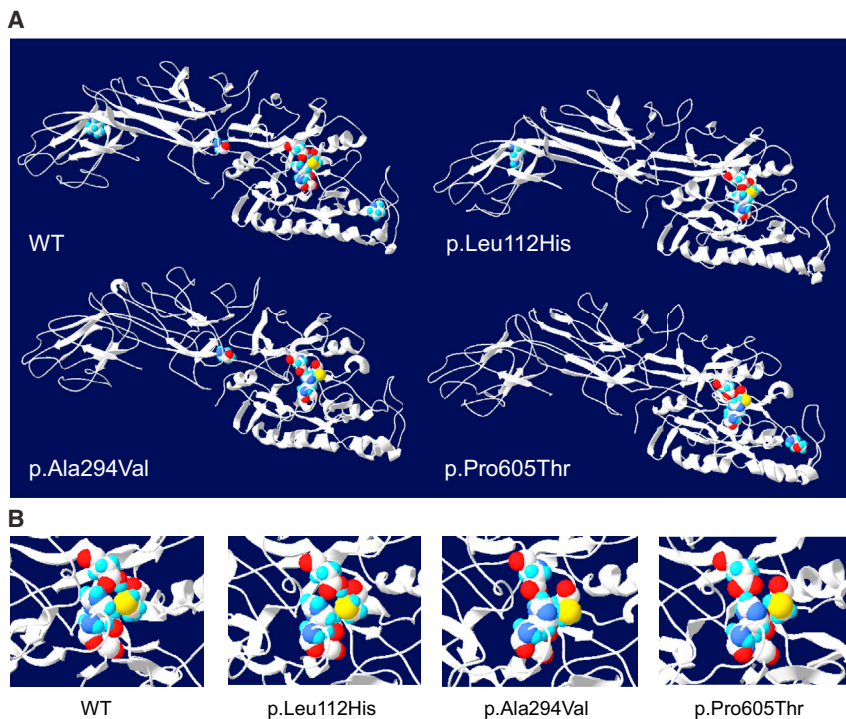


Figure 3. Topological Tridimensional Models of WT and Mutant PADI3

(A) Overall view of the tridimensional solid-ribbon representation of calcium-bound WT and three mutant PADI3 models. The tridimensional solid residues Leu112, Ala294, and Pro605, with their respective lateral chains, are reported on the proposed model of the WT enzyme, as well as the corresponding substituted amino acids on the model of each mutant, p.Leu112His, p.Ala294Val, and p.Pro605Thr. The four amino acids involved in the catalytic site are also shown. According to these models, the p.Ala294Val and p.Pro605Thr substitutions induce a profound disorganization of the predicted immunoglobulin-like domains, with disappearance of several β sheets and modification of some α helices of the catalytic domain as compared to the WT. The effect of the p.Leu112His substitution is more discrete.

(B) Zoomed view of the major amino acids involved in the catalytic site. Its proposed structure is clearly modified after p.Ala294Val and p.Pro605Thr substitutions. It should be noted that none of the substituted amino acids are directly involved in this site.

to any disorder until now. *TGM3* encodes transglutaminase 3, a member of the transglutaminase family (Enzyme Commission: EC.2.3.2.13), which catalyzes the calcium-dependent formation of isopeptide bonds between glutamine and lysine residues in various proteins including the archetypal hair shaft protein trichohyalin, encoded by *TCHH*. *TCHH* is a structural protein co-localized with PADI3 in the inner root sheath of the hair follicle and in the medulla of the hair shaft. Deimination by PADI3 reduces the overall charge of *TCHH*, and that enables its association with the keratin intermediate filaments (KIF). Then, *TCHH* and KIF are crosslinked together by TGM3. KIFs are then stabilized, hardened, and linked to cornified envelopes through further crosslinking by transglutaminases, particularly by TGM3 (Figure 2H).^{30–32} Thereby, *TCHH* and its sequential modifications by PADI3 and TGM3 have a very important role in shaping and mechanical strengthening of the hair. Of note, the *TCHH* mutation we identified leads to the synthesis, if any, of a very short protein, probably without any function in KIF interaction, as the KIF interacting domain would be almost entirely missing (Figure 2G).

Missense Mutations in *PADI3* Affect the 3D Enzyme Structure

We next investigated the consequences of *PADI3* mutations on the corresponding proteins. The p.Lys578* is expected to induce the synthesis of a truncated protein lacking the 87 amino acids of the carboxyl terminus, in particular the Cys646 (Figure 2C, Table S6) absolutely necessary for the enzyme activity.²⁸ Intriguingly, we

observed that the three PADI3 amino acids substituted as a result of the missense mutations correspond to residues that are conserved in the five human PADI proteins, and also in the PADI3 from other species, suggesting that they have an important role (Figure S3). However, none of them is directly involved in the catalytic site or in one of the five calcium-binding sites of PADI3 (Table S6). Nevertheless, when we analyzed the effect of the *PADI3* missense mutations on the predicted three-dimensional structure of the enzyme,¹⁵ the mutations p.Ala294Val and p.Pro605Thr were shown to induce clear modifications of β sheets and α helices, in particular in the immunoglobulin-like NH2 domains, and also around the catalytic site and the calcium-binding sites. The effects of the p.Leu112His substitution were less drastic (Figures 3, S4, and S5).

Aggregation and Reduced Enzymatic Activity of PADI3 Mutants

We then cloned the WT *PADI3* cDNA into a mammalian expression vector in order to induce the translation of a C-terminally V5-tagged PADI3 protein. Mutant constructs with the three recurrent missense mutations were generated by targeted mutagenesis. HaCaT cells were transiently transfected (5%–10% transfection efficiency) with constructs encoding for WT and mutant forms of PADI3. Immunoblotting of cell extracts showed that all of the constructs led to translation of a protein of about 70 kDa (Figure 4A). The subcellular location of WT and mutated proteins was determined by immunofluorescence analyses that showed, as expected, a diffuse homogeneous

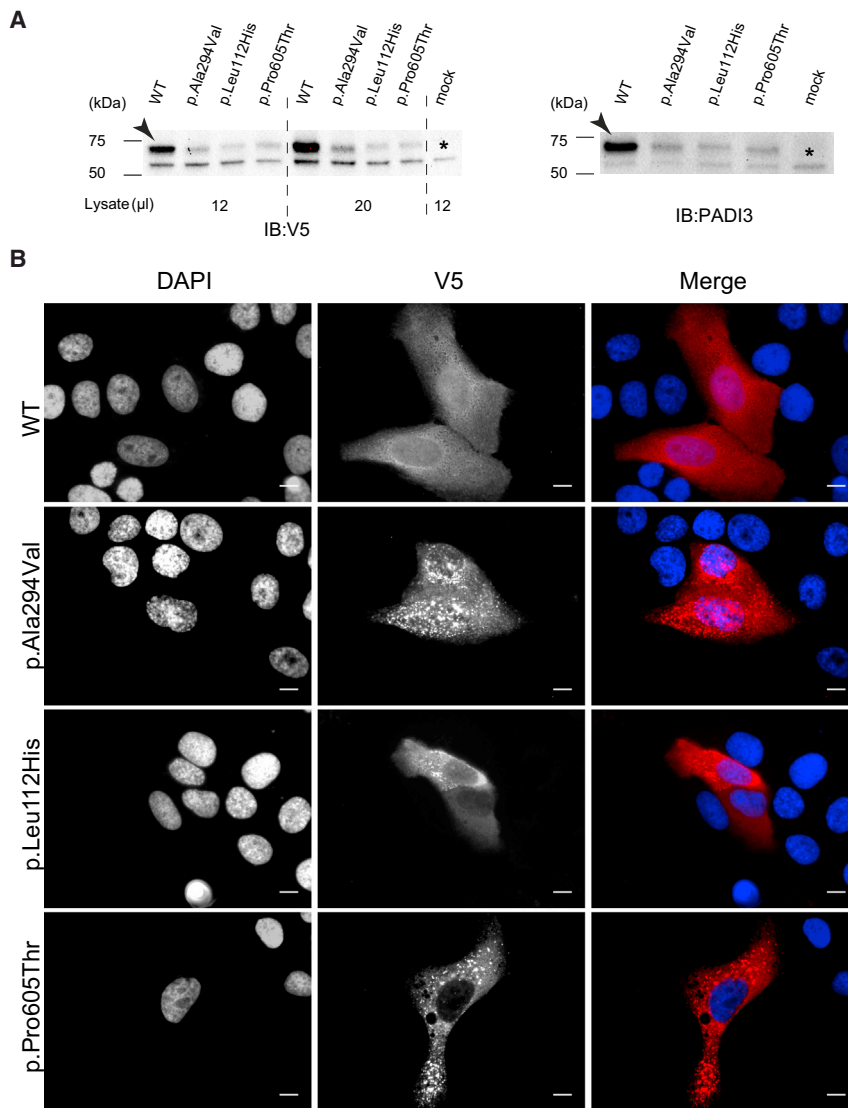


Figure 4. WT and Mutant Forms of PADI3 Produced in HaCaT Cell Line

(A) Immunoblotting analysis shows the translation of WT and mutant PADI3 in transiently transfected HaCaT cells, which were collected 48 hr after transfection. Immunoblotting was performed with anti-V5 and anti-PADI3 antibodies. Antibody-specific bands are indicated with an arrow and a non-specific cross-reactive band around 55 kDa is indicated with an asterisk. Full-length blot images can be seen in Figure S9.

(B) Immunofluorescence analysis in HaCaT cells transiently transfected with WT and mutant PADI3 encoding plasmids shows the homogeneous cytosolic localization of WT PADI3 whereas the three mutant proteins are observed in the form of large aggregates. Scale bars represent 10 µm.

Padi3 Knockout Mice Show Whisker and Hair Anomalies

In order to demonstrate the importance of PADI3 in hair shaft formation and structure, we generated *Padi3* knockout mice (Figures 6A and 6B). Breeding mice heterozygous for the *Padi3*^{tm1a} mutation produced offspring with the three possible genotypes at the expected Mendelian ratios, showing that absence of *Padi3* is compatible with life. Grossly, the skin of 7-week-old null mice appeared normal. A further characterization by SEM revealed alterations in the morphology of hair coat (Figure 6C) and, less markedly, of whiskers. The surface of the lower (proximal) part of the vibrissae and the hairs on their entire length were irregular and rough and appeared as if hammered.

Nonsense Mutation in TGM3 Leads to Reduced Enzymatic Activity

We cloned the WT *TGM3* cDNA into a mammalian expression vector in order to induce the translation of an N-terminally FLAG-tagged TGM3 protein. Mutant construct was generated by targeted mutagenesis. HaCaT and HEK293T cell lines were transiently transfected with WT and mutant TGM3 encoding constructs. WT TGM3 construct led to translation of a protein of about 70 kDa, while the nonsense mutation resulted in a truncated protein of around 40 kDa with a lower detection level (Figures 7A and S7). Immunofluorescence analysis showed that TGM3 is located in the cytoplasm and that the truncated form is present in a dramatically lower number of cells (Figure 7B) in accordance with the western blot results. Generally these cells had a smaller cytosolic surface area in comparison to those producing the WT TGM3

cytoplasmic distribution of the WT PADI3,²² whereas in all three mutants the proteins were observed to form large aggregates throughout the cytoplasm (Figure 4B). To assess the enzymatic activity of WT and mutated PADI3, we performed double immunostaining with an anti-V5 monoclonal antibody and with human anti-citrullinated protein autoantibodies (ACPA) from individuals with rheumatoid arthritis, these antibodies specifically detecting citrullinated proteins.^{18,33} Although translation of the WT PADI3 resulted in a strong labeling with the ACPA antibodies, the signal in the cells producing the mutant proteins was barely above background (Figure 5A). We also produced the WT and mutant PADI3 in *E. coli*. After incubation of the WT PADI3-containing bacterial extracts with calcium for 2 hr, deiminated proteins were detected. By contrast, when the extracts containing the mutated PADI3 were incubated for 2 hr, and even up to 18 hr, no deiminated proteins were detected (Figures 5B and S6). Altogether, the results suggested that the mutated forms of PADI3 are either not or only weakly active.

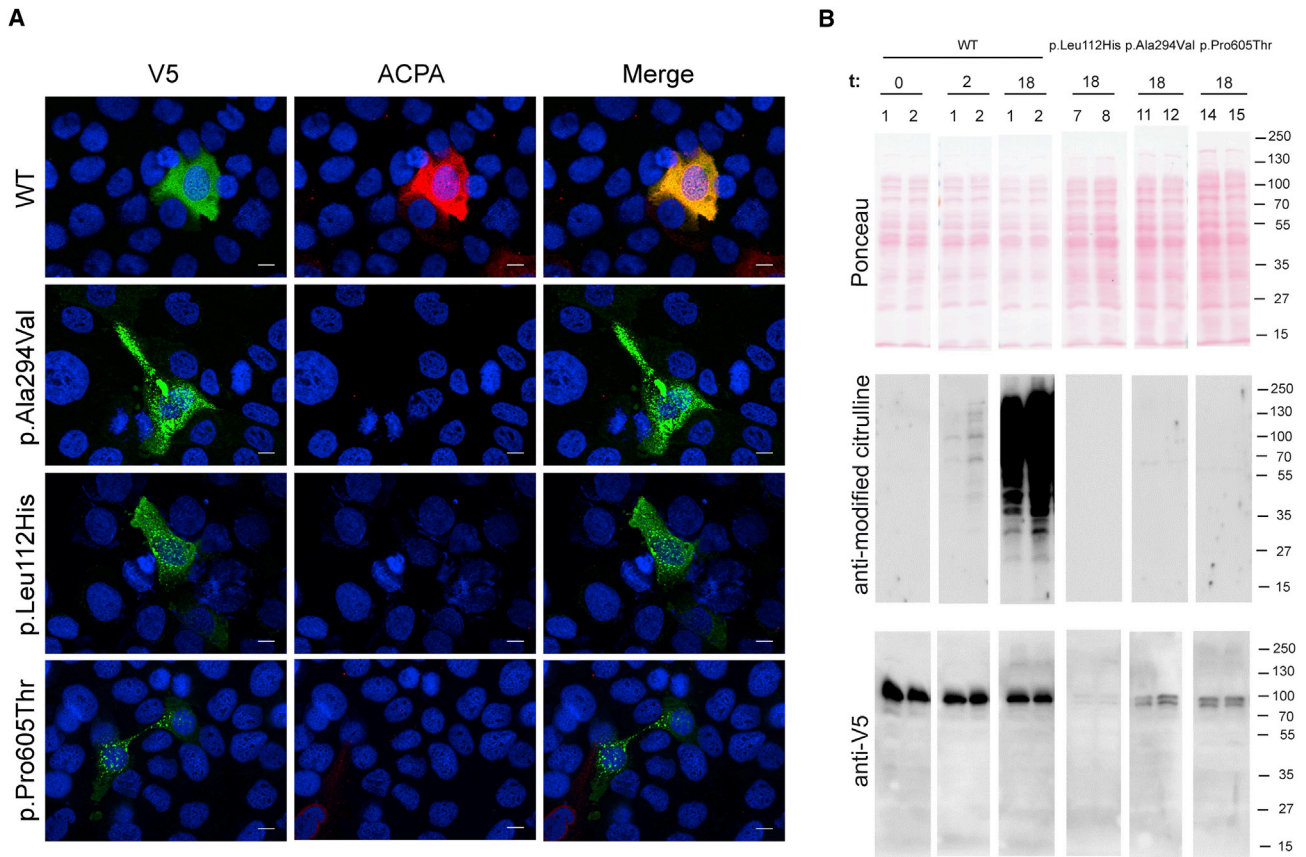


Figure 5. Consequences of *PADI3* Mutations on the Enzyme Activity

(A) Indirect immunofluorescence analysis of transfected HaCaT cells. HaCaT cells were double labeled with anti-V5 monoclonal antibody (green) and ACPA antibodies (red). Nuclei were labeled with DAPI (blue). Scale bars represent 10 μ m. The WT *PADI3* is clearly active (merge image; yellow color) whereas the mutants display a low activity.

(B) WT *PADI3* (bacterial clones 1 and 2) and the mutant forms, p.Leu112His (clones 7 and 8), p.Ala294Val (clones 11 and 12), and p.Pro605Thr (clones 14 and 15), produced in *E. coli*, were extracted in Tris-HCl buffered salt. Soluble proteins were incubated for the indicated period of time (t; in hours) with calcium, separated by electrophoresis, transferred to membranes, stained with Ponceau Red, and immunodetected with either the anti-modified citrulline rabbit antibodies or anti-V5 antibody. Although citrullinated proteins were detected when the WT-containing extracts have been incubated for 2 hr, no citrullinated proteins were detected in the mutant-containing extracts, even after 18 hr of incubation. The substituted enzymes appear to be cleaved and a V5-reactive doublet is observed. Molecular mass markers are indicated on the right in kDa. Full-length blot images can be seen in Figure S9.

(Figure 7B). We performed a transglutaminase activity assay²³ with HEK293T cell lysates containing WT and mutated TGM3. The analysis results revealed that the WT had a significantly higher transglutaminase activity in comparison to the truncated protein and the latter did not differ from the mock transfected negative control (Figures 7C and S8).

Discussion

In this study we identified disease-causative mutations for UHS in *PADI3*, *TGM3*, and *TCHH*, with the former two genes encoding for posttranslational modification enzymes that act on the structural hair protein trichohyalin encoded by the latter gene. Our cell culture data show that the identified mutations in *PADI3* and *TGM3* lead to reduced or no enzymatic activity and the phenotype of the *Padi3* knockout mice we generated show structural alterations in

the whiskers and hair coat morphology. Our findings are also supported by the phenotype of the already existing *Tgm3* knockout mice. These mice exhibit irregular, twisted whiskers and, at birth, have a wavy hair coat, which improves 4 weeks after birth.³⁴ Scanning and transmission electron microscopy analyses of hairs from adult *Tgm3*^{-/-} mice reveal alterations such as irregular torsions, deformed grooves, abnormal cuticle, and shorter KIF.³⁴ It is also convincing that both nonsense and missense mutations in *Tgm3* are responsible for the wellhaairig mouse phenotype, named for the curly whiskers and wavy coat of the mutant animals.³⁵ Based on the phenotype of the *Tgm3*^{-/-} mice, John et al. have suggested that alterations in TGM3 or its substrates could be related to recessive forms of pili torti (MIM: 261900) or similar hair phenotypes, which improve with age.³⁴ Our findings validate this hypothesis and furthermore identify UHS as the hair phenotype related to alterations not only in TGM3 but also in the other proteins of the TCHH-*PADI3*-TGM3 cascade. In

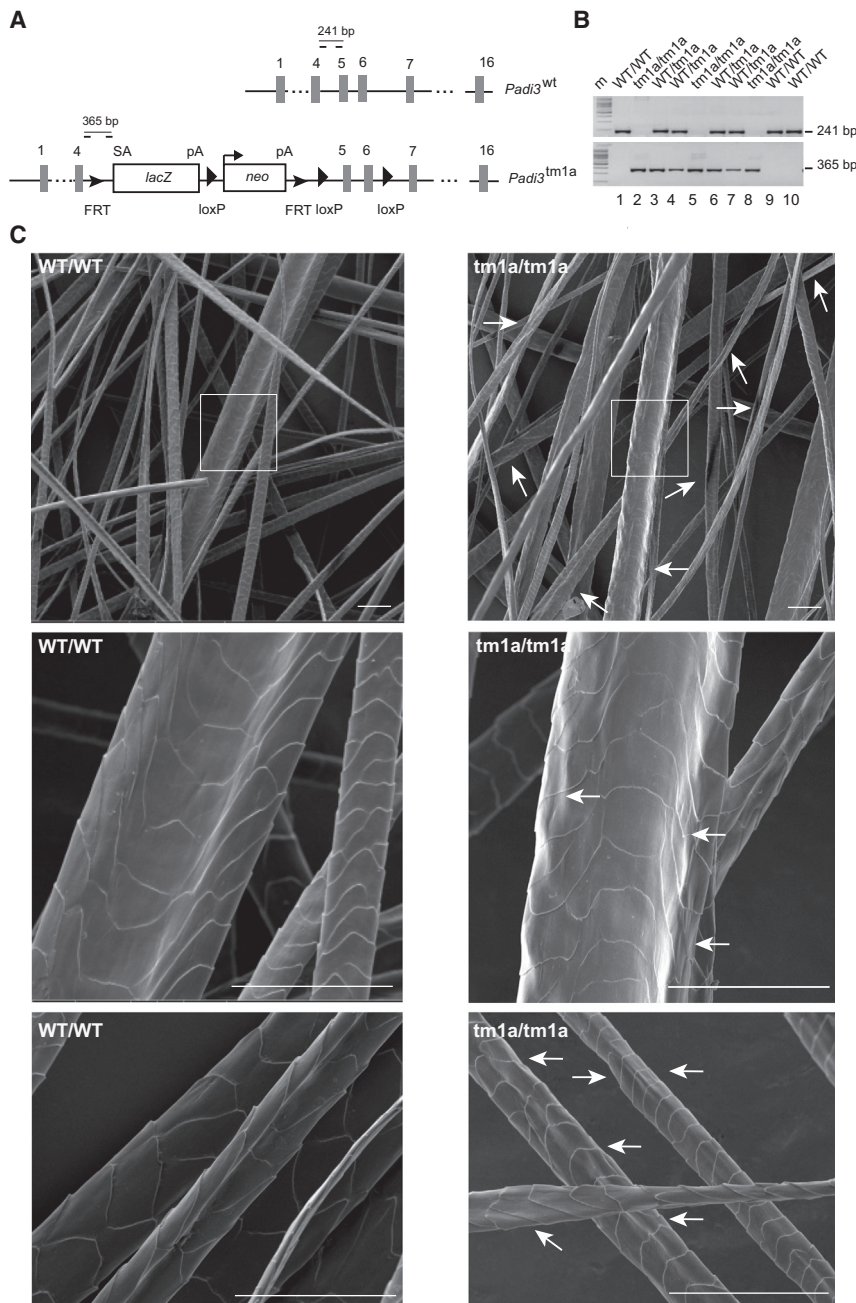


Figure 6. *Padi3* Gene Disruption in Mice

(A) Schematic representation of *Padi3* and the targeting vector. The exons are shown by numbered gray rectangles. A cassette containing the beta-galactosidase (*LacZ*) and neomycin (*neo*) genes is inserted between exons 4 and 5. This results in the production of a truncated *Padi3* protein corresponding to amino acids 1–136 fused to β-galactosidase. The position of the inserted loxP and flippase recognition target (FRT) sites are indicated, as well as the splicing acceptor site (SA) and the polyadenylation sites (pA) of *LacZ* and *neo*. The positions of the oligonucleotides (dashes) used for genotyping are shown, as well as the length of the amplified PCR products in wild-type (*Padi3*^{wt}) and targeted (*Padi3*^{tm1a}) alleles. (B) PCR on genomic DNA from tail biopsies of ten mice from the same littermate (five females [1–5] and five males [6–10]) showing amplification of the 241 bp fragment for the *Padi3*^{wt} allele and the 365 bp fragment for the *Padi3*^{tm1a} allele.

(C) Representative pictures of SEM analysis of back hair coat from the three WT and three *Padi3*^{tm1a/tm1a} mice (7 weeks old). Most hairs of the knockout mice are rough, with an irregular surface (white arrows). This is evident for thick hairs (top and middle micrographs) but was also observed for thin hairs (bottom). In some cases the hairs are twisted. The boxed areas are enlarged in the middle. At least 6 vibrissae and 200 hairs were analyzed per animal. Scale bars represent 50 μm.

some affected individuals, TCHH would not be produced, or produced as a truncated form unable to interact with KIF; in others, because of a PADI3 activity defect, TCHH would remain insoluble, preventing its interaction with KIF; in the last group, TCHH/KIF interaction would not be stabilized by TGM3-mediated crosslinks. Taken together, this suggests that one of the particular processes in hair shaft formation that leads to UHS when disturbed might be the interaction of TCHH and KIF. This interaction is known to be crucial for shaping and mechanical strengthening of the hair shaft. These findings also show that the compromise of any one of the proteins that play a role in this process would be enough to lead to the same phenotype.

It is intriguing that, despite the defects affecting a structural component of the hair shaft, the phenotype in UHS is commonly reported to improve with age, similar to the hair coat phenotype of *Tgm3*^{-/-} mice. Interestingly, improvement with age has also been observed in other hair shaft disorders (e.g., pili annulati, pili torti). The improvement in UHS might be due to the compensatory expression of

another isoform of peptidylarginine deiminase, transglutaminase, or other structural hair shaft components. On the other hand, aging-related changes in hair follicles such as increase in diameter and length can have mechanistic influences that might account for this improvement. TGM3 and PADI3 are strongly detected in the upper epidermis. Nevertheless, no anomalies have been reported in the interfollicular epidermis of individuals with isolated UHS. Similarly, *Tgm3*^{-/-} mice show no obvious skin defects.³⁴ This is probably due to the fact that other isoforms of these enzyme families are present in the epidermis, which can compensate for the loss of PADI3 and TGM3 activity, whereas these two are the only isoforms detected in the hair cuticles and medulla.^{27,28,30}

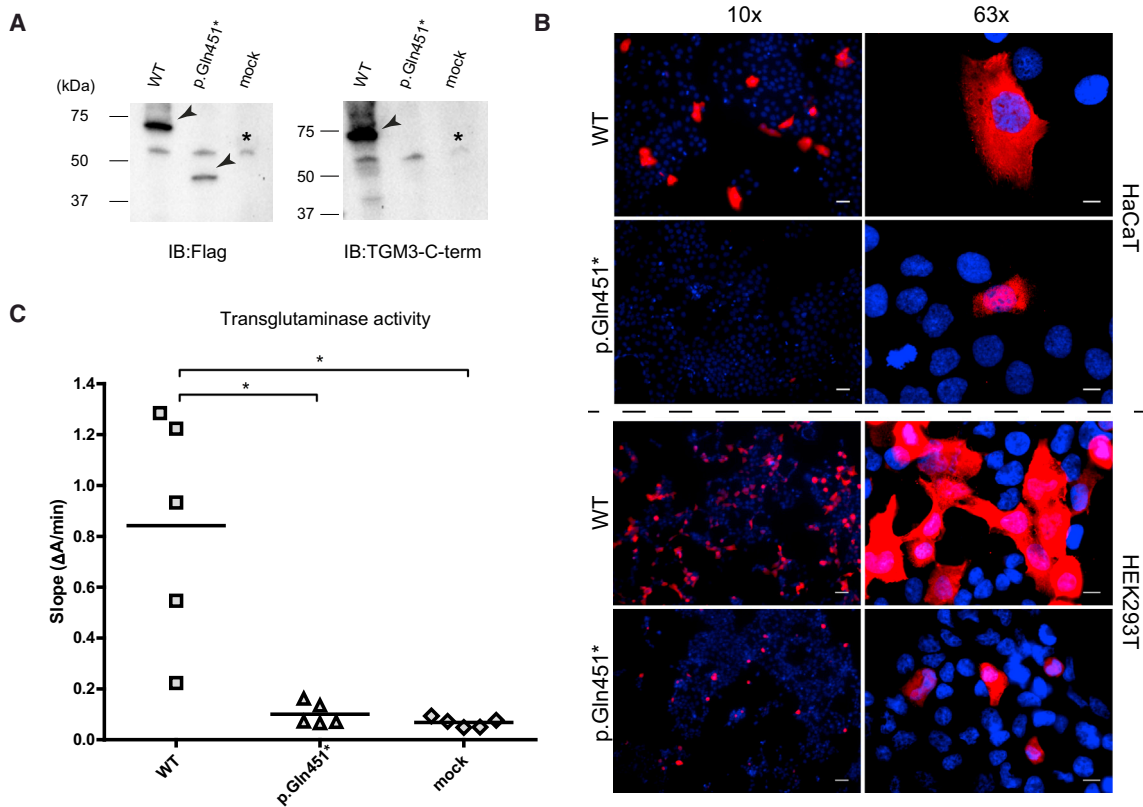


Figure 7. WT and Mutant Forms of TGM3 Produced in HaCaT and HEK293T Cell Lines

(A) Immunoblotting analysis shows the translation of WT and truncated TGM3 in transiently transfected HaCaT cells, collected 48 hr post-transfection. Immunoblotting was performed with anti-Flag and anti-TGM3 antibodies. Antibody-specific bands showing the WT (~70 kDa) and truncated TGM3 (~40 kDa) are indicated with an arrow and a non-specific cross-reactive band around 55 kDa is indicated with an asterisk. The truncated TGM3 can be detected only with the antibody against the Flag epitope fused to the N terminus and not with the antibody against the C terminus of TGM3 as expected. Full-length blot images can be seen in [Figure S9](#). Immunoblotting analysis with HEK293T cells is presented in [Figure S7](#).

(B) Immunofluorescence analyses in HaCaT and HEK293T cells transiently transfected with WT and mutant TGM3 encoding constructs are presented by images captured with 10 \times and 63 \times objectives. The analyses show clear differences in the number of cells producing the WT and mutant TGM3 (10 \times images). Scale bars represent 50 μ m and 10 μ m for 10 \times and 63 \times objectives, respectively.

(C) Transglutaminase activity of WT and mutant TGM3 produced in HEK293T cells. Mock-transfected cell lysates were used as negative control. The transglutaminase activity, represented by the mean slope of 10 min long measurements from technical triplicates (given in [Figure S8](#)), is presented as a dot plot. The enzymatic activity assay was performed with samples emerging from five independent transfections. Horizontal lines represent the mean values (mean \pm SD; WT, 0.84 \pm 0.45; p.Gln451*, 0.10 \pm 0.04; mock, 0.07 \pm 0.02). Results demonstrate that the mutated protein did not differ from the mock transfected negative control in terms of activity and WT TGM3 had a significantly higher activity in comparison to both (* p < 0.05, Dunn's test).

Up to now, both simplex and familial cases of UHS have been reported with suggested autosomal-dominant and -recessive inheritance with variable levels of penetrance. In this study we consistently observed an autosomal-recessive inheritance pattern in a total of 11 familial and simplex cases. Based on the pedigrees reported in literature, it is most likely that autosomal-dominant forms of this condition exist^{7,36,37} which might be underlined by defects in other genes involved in hair shaft formation and maintenance related processes. It would be of interest then to investigate closely whether differences could be observed in the phenotypes of these individuals in comparison to the individuals who carry recessive mutations in *PADI3*-*TCHH*-*TGM3* cascade.

An interesting observation was that 5 out of 60,659 individuals in ExAC are homozygous for c.881C>T

(p.Ala294Val). UHS is a non-debilitating phenotype that resolves with age and therefore, it is likely that these presumably affected individuals had participated in the ExAC project as "healthy" controls. These data also indicate that UHS is a more common phenotype than estimated.

In summary, we elucidated the molecular genetic background of UHS by identifying recessive mutations in *PADI3*, *TCHH*, and *TGM3*. The three genes encode for proteins that play an essential role during hair shaft formation through their sequential interactions. This finding, in combination with the data describing the functional effects of the mutations in *PADI3* and *TGM3*, provides valuable information regarding the pathophysiology of UHS. Furthermore, it contributes to a better understanding of the protein interaction cascades in molecular histogenesis of the hair. This could be of further value for cosmetic and

pharmaceutic industries paving the way for development of novel products.

Supplemental Data

Supplemental Data include nine figures and six tables and can be found with this article online at <http://dx.doi.org/10.1016/j.ajhg.2016.10.004>.

Acknowledgments

P.N. is a founder, CEO, and shareholder of ATLAS Biolabs GmbH, which is a service provider for genomic analyses. We would like to thank the individuals and their families for participating in this study. We would like to acknowledge Dr. Marianne Chabod, the technical assistance of Carole Pons and Géraldine Offer, the Toulouse Rio Imagerie imaging (INSERM U1043) and electron microscopy (University of Toulouse) facilities, and the TAMM animal facility, in particular Laëtitia Trottereau. We would like to thank Dr. Thomas Zillinger for providing us with HEK293T cells. We would like to acknowledge Dr. Thomas Butterbrodt from Bio-Rad Laboratories GmbH and Dr. Kourosh Zolghadr from Leica Biosystems for their technical assistance. S.S. is supported by the Deutsche Forschungsgemeinschaft (DFG, SFB1089), the German Ministry of Research and Education (BMBF, 01GQ0806), and the European Union's Seventh Framework Programme (FP7/2007-2013) under grant agreement number 602102 (EPITARGET). V.O. is supported by the German Research Foundation (DFG) (OJ 53/3-1). M.S. and G.S. are supported by The University of Toulouse, the Centre National de la Recherche Scientifique, and the Institut National de la Santé et de la Recherche Médicale. This work was further supported by local funding (BONFOR to R.C.B. and S.S.). R.C.B. is a member of the DFG-funded Excellence Cluster ImmunoSensation and was a recipient of a Heisenberg Professorship of the DFG (BE 2346/4-2).

Received: September 12, 2016

Accepted: October 5, 2016

Published: November 17, 2016

Web Resources

BLAST, <http://blast.ncbi.nlm.nih.gov/Blast.cgi>
Enzyme Commission, <http://www.chem.qmul.ac.uk/iubmb/enzyme/>
ExAC Browser (accessed 5 March 2015), <http://exac.broadinstitute.org/>
GenBank, <http://www.ncbi.nlm.nih.gov/genbank/>
International Mouse Phenotyping Consortium, <http://www.mousephenotype.org/data/genes/>
OMIM, <http://www.omim.org/>
RCSB Protein Data Bank, <http://www.rcsb.org/pdb/home/home.do>
RRID, <https://scicrunch.org/resources>
varbank, <https://varbank.ccg.uni-koeln.de>
UCSC Human Genome Browser, <http://genome.ucsc.edu/cgi-bin/hgGateway>

References

1. Dupré, A., Rochiccioli, P., and Bonafé, J.L. (1973). Cheveux incoiffables: anomalie congénitale des cheveux. *Bull. Soc. Fr. Dermatol. Syphiligr.* *80*, 111–112.
2. Stroud, J.D., and Mehregan, A.H. (1973). *The First Human Hair Symposium* (New York: Medcom Press).
3. Calderon, P., Otberg, N., and Shapiro, J. (2009). Uncombable hair syndrome. *J. Am. Acad. Dermatol.* *61*, 512–515.
4. Trüeb, R.M., Spycher, M.A., Schumacher, F., and Burg, G. (1994). [Pili torti et canaliculi in ectodermal dysplasia]. *Hautarzt* *45*, 372–377.
5. Navarini, A.A., Kaufmann, F., Kaech, A., Trüeb, R.M., and Weibel, L. (2010). Picture of the month. Uncombable hair (pili trianguli et canaliculi). *Arch. Pediatr. Adolesc. Med.* *164*, 1165–1166.
6. Ferrando, J., Fontarnau, R., Gratacos, M.R., and Mascaro, J.M. (1980). [Pili canaliculi (uncombable hair syndrome or spun glass hair syndrome). A scanning electron microscope study of ten new cases (author's transl)]. *Ann. Dermatol. Venereol.* *107*, 243–248.
7. Hebert, A.A., Charrow, J., Esterly, N.B., and Fretzin, D.F. (1987). Uncombable hair (pili trianguli et canaliculi): evidence for dominant inheritance with complete penetrance based on scanning electron microscopy. *Am. J. Med. Genet.* *28*, 185–193.
8. Mallon, E., Dawber, R.P., De Berker, D., and Ferguson, D.J. (1994). Cheveux incoiffables—diagnostic, clinical and hair microscopic findings, and pathogenic studies. *Br. J. Dermatol.* *131*, 608–614.
9. Hicks, J., Metry, D.W., Barrish, J., and Levy, M. (2001). Uncombable hair (cheveux incoiffables, pili trianguli et canaliculi) syndrome: brief review and role of scanning electron microscopy in diagnosis. *Ultrastruct. Pathol.* *25*, 99–103.
10. Shelley, W.B., and Shelley, E.D. (1985). Uncombable hair syndrome: observations on response to biotin and occurrence in siblings with ectodermal dysplasia. *J. Am. Acad. Dermatol.* *13*, 97–102.
11. Li, H., and Durbin, R. (2009). Fast and accurate short read alignment with Burrows-Wheeler transform. *Bioinformatics* *25*, 1754–1760.
12. McKenna, A., Hanna, M., Banks, E., Sivachenko, A., Cibulskis, K., Kernysky, A., Garimella, K., Altshuler, D., Gabriel, S., Daly, M., and DePristo, M.A. (2010). The Genome Analysis Toolkit: a MapReduce framework for analyzing next-generation DNA sequencing data. *Genome Res.* *20*, 1297–1303.
13. Li, H., Handsaker, B., Wysoker, A., Fennell, T., Ruan, J., Homer, N., Marth, G., Abecasis, G., and Durbin, R.; 1000 Genome Project Data Processing Subgroup (2009). The Sequence Alignment/Map format and SAMtools. *Bioinformatics* *25*, 2078–2079.
14. Boukamp, P., Petrussevska, R.T., Breitkreutz, D., Hornung, J., Markham, A., and Fusenig, N.E. (1988). Normal keratinization in a spontaneously immortalized aneuploid human keratinocyte cell line. *J. Cell Biol.* *106*, 761–771.
15. Méchin, M.C., Coudane, F., Adoue, V., Arnaud, J., Duplan, H., Charveron, M., Schmitt, A.M., Takahara, H., Serre, G., and Simon, M. (2010). Deimination is regulated at multiple levels including auto-deimination of peptidylarginine deiminases. *Cell. Mol. Life Sci.* *67*, 1491–1503.
16. Arita, K., Hashimoto, H., Shimizu, T., Nakashima, K., Yamada, M., and Sato, M. (2004). Structural basis for Ca(2+)-induced activation of human PAD4. *Nat. Struct. Mol. Biol.* *11*, 777–783.
17. Posch, A., Kohn, J., Oh, K., Hammond, M., and Liu, N. (2013). V3 stain-free workflow for a practical, convenient, and reliable total protein loading control in western blotting. *J. Vis. Exp.* *82*, 50948.

18. Masson-Bessière, C., Sebbag, M., Girbal-Neuhausser, E., Nogueira, L., Vincent, C., Senshu, T., and Serre, G. (2001). The major synovial targets of the rheumatoid arthritis-specific antifilaggrin autoantibodies are deiminated forms of the alpha- and beta-chains of fibrin. *J. Immunol.* *166*, 4177–4184.
19. Anquetil, F., Clavel, C., Offer, G., Serre, G., and Sebbag, M. (2015). IgM and IgA rheumatoid factors purified from rheumatoid arthritis sera boost the Fc receptor- and complement-dependent effector functions of the disease-specific anti-citrullinated protein autoantibodies. *J. Immunol.* *194*, 3664–3674.
20. Méchin, M.C., Enji, M., Nachat, R., Chavanas, S., Charveron, M., Ishida-Yamamoto, A., Serre, G., Takahara, H., and Simon, M. (2005). The peptidylarginine deiminases expressed in human epidermis differ in their substrate specificities and subcellular locations. *Cell. Mol. Life Sci.* *62*, 1984–1995.
21. Senshu, T., Akiyama, K., Kan, S., Asaga, H., Ishigami, A., and Manabe, M. (1995). Detection of deiminated proteins in rat skin: probing with a monospecific antibody after modification of citrulline residues. *J. Invest. Dermatol.* *105*, 163–169.
22. Nachat, R., Méchin, M.C., Takahara, H., Chavanas, S., Charveron, M., Serre, G., and Simon, M. (2005). Peptidylarginine deiminase isoforms 1-3 are expressed in the epidermis and involved in the deimination of K1 and filaggrin. *J. Invest. Dermatol.* *124*, 384–393.
23. Aufenvenne, K., Oji, V., Walker, T., Becker-Pauly, C., Hennies, H.C., Stöcker, W., and Traupe, H. (2009). Transglutaminase-1 and bathing suit ichthyosis: molecular analysis of gene/environment interactions. *J. Invest. Dermatol.* *129*, 2068–2071.
24. Nissen, C.V., and Svendsen, M.T. (2013). [Uncombable hair syndrome]. *Ugeskr. Laeger* *175*, 2878.
25. Novoa, A., Azon, A., and Grimalt, R. (2012). Síndrome del pelo impenable. Uncombable hair syndrome. *Ann. Pediatr. (Paris)* *77*, 139–140.
26. Kiliç, A., Oğuz, D., Can, A., Akil, H., and Gürbüz Köz, O. (2013). A case of uncombable hair syndrome: light microscopy, trichoscopy and scanning electron microscopy. *Acta Dermatovenerol. Croat.* *21*, 209–211.
27. Kanno, T., Kawada, A., Yamanouchi, J., Yosida-Noro, C., Yoshiki, A., Shiraiwa, M., Kusakabe, M., Manabe, M., Tezuka, T., and Takahara, H. (2000). Human peptidylarginine deiminase type III: molecular cloning and nucleotide sequence of the cDNA, properties of the recombinant enzyme, and immunohistochemical localization in human skin. *J. Invest. Dermatol.* *115*, 813–823.
28. Méchin, M.C., Sebbag, M., Arnaud, J., Nachat, R., Foulquier, C., Adoue, V., Coudane, F., Duplan, H., Schmitt, A.M., Chavanas, S., et al. (2007). Update on peptidylarginine deiminases and deimination in skin physiology and severe human diseases. *Int. J. Cosmet. Sci.* *29*, 147–168.
29. Takahara, H.S.G., and Simon, M. (2014). Deimination in skin and regulation of peptidyl-arginine deiminase expression in keratinocytes. In *Protein Deimination in Health and Disease*, A. Nicholas, ed. (New York: Springer), pp. 113–128.
30. Steinert, P.M., Parry, D.A., and Marekov, L.N. (2003). Trichohyalin mechanically strengthens the hair follicle: multiple cross-bridging roles in the inner root sheath. *J. Biol. Chem.* *278*, 41409–41419.
31. Tarcsa, E., Marekov, L.N., Andreoli, J., Idler, W.W., Candi, E., Chung, S.I., and Steinert, P.M. (1997). The fate of trichohyalin. Sequential post-translational modifications by peptidyl-arginine deiminase and transglutaminases. *J. Biol. Chem.* *272*, 27893–27901.
32. Westgate, G.E., Botchkareva, N.V., and Tobin, D.J. (2013). The biology of hair diversity. *Int. J. Cosmet. Sci.* *35*, 329–336.
33. Vincent, C., Nogueira, L., Clavel, C., Sebbag, M., and Serre, G. (2005). Autoantibodies to citrullinated proteins: ACPA. *Autoimmunity* *38*, 17–24.
34. John, S., Thiebach, L., Frie, C., Mokkaapati, S., Bechtel, M., Nischt, R., Rosser-Davies, S., Paulsson, M., and Smyth, N. (2012). Epidermal transglutaminase (TGase 3) is required for proper hair development, but not the formation of the epidermal barrier. *PLoS ONE* *7*, e34252.
35. Brennan, B.M., Huynh, M.T., Rabah, M.A., Shaw, H.E., Bisailon, J.J., Radden, L.A., 2nd, Nguyen, T.V., and King, T.R. (2015). The mouse wellhaarig (we) mutations result from defects in epidermal-type transglutaminase 3 (Tgm3). *Mol. Genet. Metab.* *116*, 187–191.
36. Garty, B., Metzker, A., Mimouni, M., and Varsano, I. (1982). Uncombable hair: a condition with autosomal dominant inheritance. *Arch. Dis. Child.* *57*, 710–712.
37. de Luna, M.M., Rubinson, R., and de Kohan, Z.B. (1985). Pili trianguli canaliculi: uncombable hair syndrome in a family with apparent autosomal dominant inheritance. *Pediatr. Dermatol.* *2*, 324–327.

Supplemental Data

Mutations in Three Genes Encoding Proteins

Involved in Hair Shaft Formation

Cause Uncombable Hair Syndrome

F. Buket Ü. Basmanav, Laura Cau, Aylar Tafazzoli, Marie-Claire Méchin, Sabrina Wolf, Maria Teresa Romano, Frederic Valentin, Henning Wiegmann, Anne Huchenq, Rima Kandil, Natalie Garcia Bartels, Arzu Kilic, Susannah George, Damian J. Ralser, Stefan Bergner, David J.P. Ferguson, Ana-Maria Oprisoreanu, Maria Wehner, Holger Thiele, Janine Altmüller, Peter Nürnberg, Daniel Swan, Darren Houniet, Aline Büchner, Lisa Weibel, Nicola Wagner, Ramon Grimalt, Anette Bygum, Guy Serre, Ulrike Blume-Peytavi, Eli Sprecher, Susanne Schoch, Vinzenz Oji, Henning Hamm, Paul Farrant, Michel Simon, and Regina C. Betz

Supplemental Note: Case Reports

Clinical data for individuals with *PADI3* mutations

The English family has also been described in the manuscript. The female sibling was referred to the Department of Dermatology in Brighton at the age of 11 years with a lump in her right and left arm. The clinical and later histological diagnosis was of pilomatrixomas. At the same appointment it was noted that she had abnormal hair. This was first noticed by the parents after 8 weeks of hair shedding in early childhood. The hair was then very slow growing, came out easily and painlessly. Her hair was hard to brush or comb and she rarely had to have her hair cut. Teeth and nail development was normal. The girl has recently been diagnosed as diabetic. Her brother was examined at the age of 15 years and had white brittle nails. His hair when long was described as being like sheeps wool which had improved with age (Figure 1J). The hair had a spangly appearance. The features of the hair shaft observed by electron microscopy were diagnostic of uncombable hair with longitudinal running ridges (Figure 1K), some twisting and triangular or heart shaped cross sections (Figure 1L).

A 3-year old Danish girl was referred for evaluation of abnormal hair (Figure 1F). Besides hair shaft anomaly she was otherwise healthy. From birth she had sparse hair until the age of 1.5 years, when the parents noted her dry and unruly hair which could not be properly combed. It was also noted that she could never grow her hair long. Hair microscopy showed hair shaft anomalies with pili canaliculi et trianguli. When she was 4 years old biotin therapy 5 mg daily was given for 6 months, which apparently improved the hair texture. Today the girl is 8 years old, and overall there has been also a spontaneous improvement of the condition (Figure 1G). This clinical signs of this girl have been described in detail elsewhere.¹

A German boy was seen at the age of 3 and 8 years with unimproved wiry hair. The blond, lusterless hair was closely cropped and irregularly stuck out from the scalp growing in lots of different directions. Of interest, the hair originating from a congenital melanocytic nevus of 2.5 x 1.5 cm size at the right temporal side of the scalp was not only darker but also appeared structurally normal without any signs of uncombability (Figure 1D).

An 18-month old Swiss boy was referred to the Department of Dermatology in Zurich for the evaluation of abnormal hair. From early infancy the parents noted dry, unruly and slow growing hair which did not maintain its shape after styling. Apart from mild obstipation he was otherwise well. No one else in the family had any similar hair problems. On examination the boy's entire scalp was observed to be covered with brown, dry, frizzy hair that projected outward and resisted any attempt to flatten it. On hair shaft microscopy longitudinal grooving and triangular cross sections were observed, consistent with pili canaliculi et trianguli. Today the boy is nearly 6 years old, and there is an improvement in the hair phenotype (Figure 1E).

A Spanish girl was seen at the age of 4 years for 'funny looking' hair. Clinical examination revealed normal brown light hair without any clear alteration on eyelashes nor eyebrows. Teeth and nails are normal. Under the scanning and optical microscope typical finding of pili canaliculi were seen. This clinical signs of this girl have been described in detail elsewhere.²

The scalp hair of a German girl was normal at birth and started to grow curly and badly combable from the age of 3 months. Hair growth was claimed to be decelerated by the mother. On clinical examination at the age of 3.5 years her shoulder-length light hair appeared dry and stood out in all directions. Hair density was not reduced, and no other abnormalities could be identified (no picture available).

Another German girl presented with very fair, uncombable hair at the age of 6 years (Figure 1B). Physical examination was within normal ranges. Until the age of 15 years the structure of the hair remained unchanged.

Another German girl was examined at the age of 4 years because of uncombable hair from infancy on (Figure 1A). Short hairstyles were preferred until spontaneous improvement occurred at the age of 10-11 years, when scalp hair gradually became more flat and easier to manage. Today, at the age of 25 years, few untamable hairs are left over in the frontal area which are straightened with hair gel.

A little German girl presented with normal hair at birth; soon after birth, the regrowing hair was noticeable, and UHS syndrome was diagnosed (Figure 1C). Nowadays, at the age of 10 years, the girl has long pretty hair that is well combable. There are no other abnormalities, a sibling has normal hair. No other individual in this family has abnormal hair structure.

Clinical data for the individual with the *TGM3* mutation

The clinical signs of this young men have recently been described elsewhere.³

Clinical data for the individual with the *TCHH* mutation

The German girl with the *TCHH* mutation came to the clinics at the age of 19 years complaining that her hair grows too slowly being otherwise healthy. Since her childhood, she had brittle, curly hair, which was barely combable. These symptoms improved until her 14th year of life.

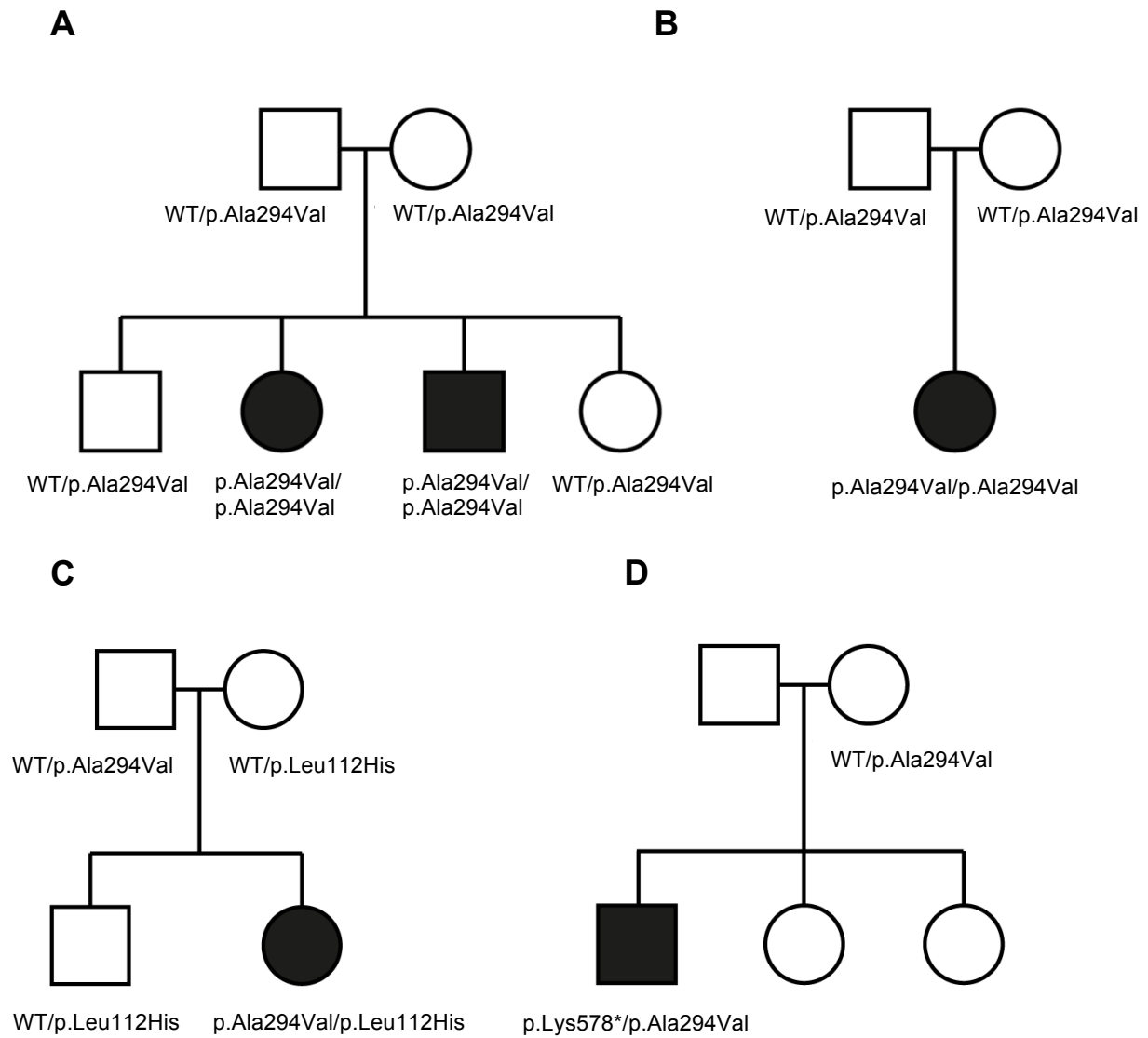


Figure S1

Co-segregation of the disease-causing mutations in pedigrees

(A) Discovery pedigree from the UK with two affected and two unaffected siblings. **(B)** Danish family with an affected daughter. **(C)** Spanish family showing compound heterozygosity for the mutations p.Leu112His and p.Ala294Val in the affected daughter. **(D)** Swiss family showing compound heterozygosity for the mutations p.Ala294Val and p.Lys578* in the affected son. DNA was not available from the healthy father and siblings. WT, wild type

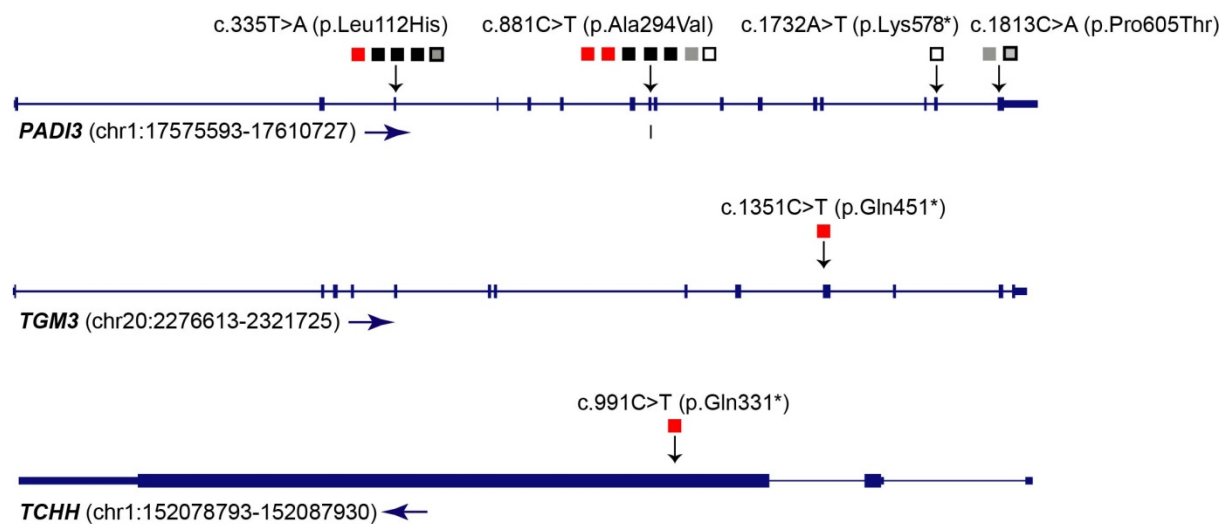
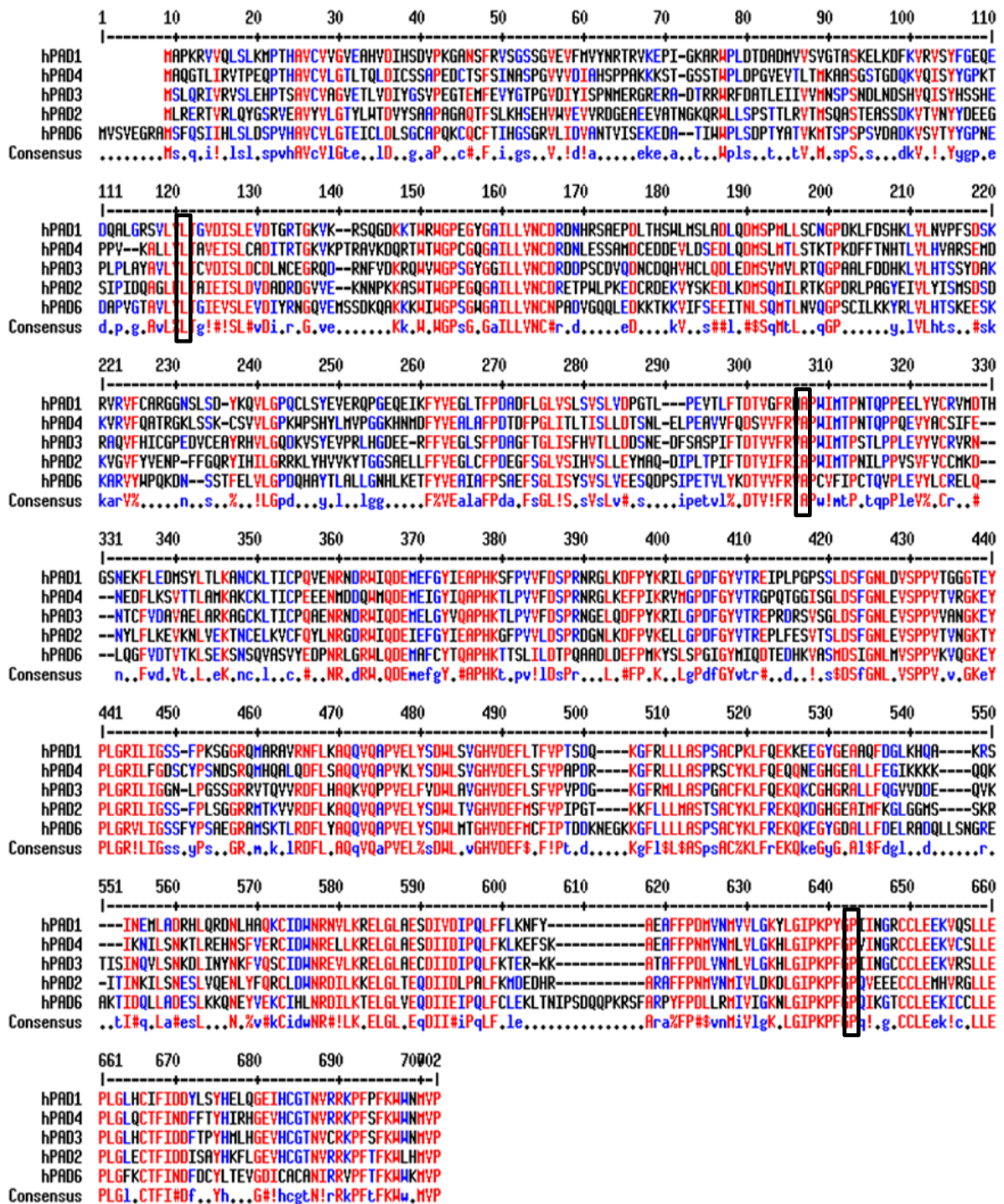


Figure S2

Cartoons depicting the positions of the mutations in *PADI3*, *TGM3* and *TCHH*

The start/end positions of the genes are based on hg19. Direction of transcription is depicted with the arrow heads. Squares indicate individuals carrying the respective mutation. Red squares denote homozygotes. Black squares denote individuals carrying p.Leu112His and p.Ala294Val, grey square denotes the individual carrying p.Ala294Val and p.Pro605Thr, grey square with a black frame denotes the individual carrying p.Leu112His and p.Pro605Thr, and white square denotes the individual carrying p.Ala294Val and p.Lys578*.

A




```

SP|Q9ULW8|PADI3_HUMAN  ISINQVLSNKDLINYNKFVQSCIDWNREVLKRELGLAECDIIDIPQLFKTER-KKATAFF 584
SP|Q9Z184|PADI3_MOUSE  VSINQILNNQSLINFNKFAQSCIDWNREVLKRELGLAEGDIIDIPQLFKTEK-RKAVAFF 584
SP|O02849|PADI3_SHEEP  VSISQVLSNGSLIGYNKFVQSCIDWNREVLKRELGLAERDIDIPQLFKMER-RKAVAFF 584
TR|G3VER6|G3VER6_SARHA MSINQILSNENLISYNKFVQSCIDWNREVLKRELGLTDRDIIDIPQLFKRER-RKAVAFF 587
TR|E2R691|E2R691_CANFA VSINQVLSNVDLISYNKFVQSCIDWNREVLKRELGLTERDIDIPQLFKTER-KKAVAFF 584
TR|F1NP39|F1NP39_CHICK PSISEILGNEALRKFNAYAQSCISWNRDILKRELGLAEQDIIDIPQLFQADHQARAVAYF 592
    **.::* * * :* :.***.***:*****.: **:* **.: : :*.**

SP|Q9ULW8|PADI3_HUMAN  PDLVNMLVLGKHLGIPKPFGPIINGCCCLEEKVRSLEPLGLHCTFIDDFTPYHMLHGEV 644
SP|Q9Z184|PADI3_MOUSE  PDLVNMLVLGKHLGIPKPFGPIINGRCCLEEKVRSLEPLGLHCTFIDDFTPYHMLHGEV 644
SP|O02849|PADI3_SHEEP  PDLVNMLVLGKHLGIPKPFGPVINGRCCLEEKVRSLEPLGLRCTFIDDFTPYHMLHGEV 644
TR|G3VER6|G3VER6_SARHA PDLVNMLVLGRHLGIPKPFGPIINGRCCLEEKVRSLEPLGLQCNFIDDFTPYHMLHGEV 647
TR|E2R691|E2R691_CANFA PDLVNMLVLGKHLGIPKPFGPIINGQCCLEEKVRSLEPLGLHCTFIDDFTPYHMLHGEV 644
TR|F1NP39|F1NP39_CHICK PDMVNMLVLGRHLGIPKPFGPLVLDGQCCLEERVALLQPLGLSCTFINDYFYSYHKLAGEV 652
    **:*****:*****.:*: * ***:**:* **:* ** * **

SP|Q9ULW8|PADI3_HUMAN  HCGTNVCRKPFSFKWWMV 664
SP|Q9Z184|PADI3_MOUSE  HCGTNVRRPFAFKWWMV 664
SP|O02849|PADI3_SHEEP  HCGTNVRRQPFSFKWWMCEP 664
TR|G3VER6|G3VER6_SARHA HCGTNVRRKPFSFKWWMIP 667
TR|E2R691|E2R691_CANFA HCGTNVRRQPFSFKWWMV 664
TR|F1NP39|F1NP39_CHICK HCGTNVRRKPFSFKWWMV 672
    ***** *:** **** * *

```

Figure S3

Sequence alignments for PADI3

When we assessed evolutionary conservation of the three substituted amino acids, we found that all of them were located **(A)** at well-conserved positions across various human PADI3s and **(B)** across PADI3 from distinct species, thus suggesting that these mutations may alter the protein function. **(A)** The sequences of human PADI3 and paralogous genes (GenBank accession numbers AB033768, AB03176, AB026831, AB017919 and AY422079) were aligned using MultAlin.⁴ Amino acids conserved at 90% and 50% are indicated in red and blue, respectively. The three mutated amino acids of PADI3 are surrounded. **(B)** Primary sequences of human PADI3 and Padi3 from other species (chicken, mouse, sheep, dog (CANFA) and Tasmanian devil (SAHRA) were aligned using Clustal Omega (European Molecular Biology Laboratory-European Bioinformatics Institute). The three mutated amino acids of PADI3 are depicted in red.

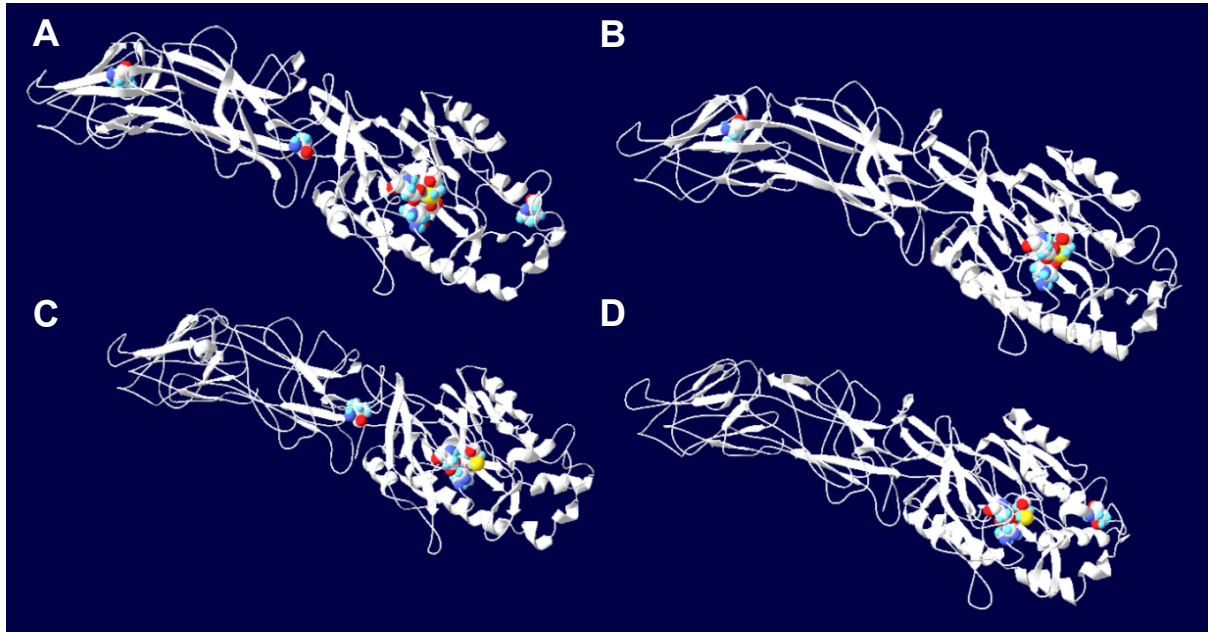


Figure S4

Topological tridimensional models of WT and mutant PADI3: Localization of the 4 major amino acids involved in the catalytic sites and of the 3 amino acids involved in the UHS missense mutations

Overall view of the tridimensional solid ribbon representation of calcium-bound PADI3 models, including WT and three missense mutants. Residues Leu112, Ala294 and Pro605 are reported on the model of the **(A)** WT enzyme, as well as the corresponding substituted amino acids on the structure of the three mutants **(B)** p.Leu112His, **(C)** p.Ala294Val and **(D)** p.Pro605Thr. **(A-D)** The four major amino acids involved in the catalytic site are also shown. According to these models, the **(C)** p.Ala294Val and **(D)** p.Pro605Thr substitutions induce a profound disorganization of the immunoglobulin-like domains, with clear disappearance of several beta-sheets, and disruption of some alpha-helices in the catalytic domain, as compared to the WT. Effects of the **(B)** p.Leu112His substitution are more discrete.

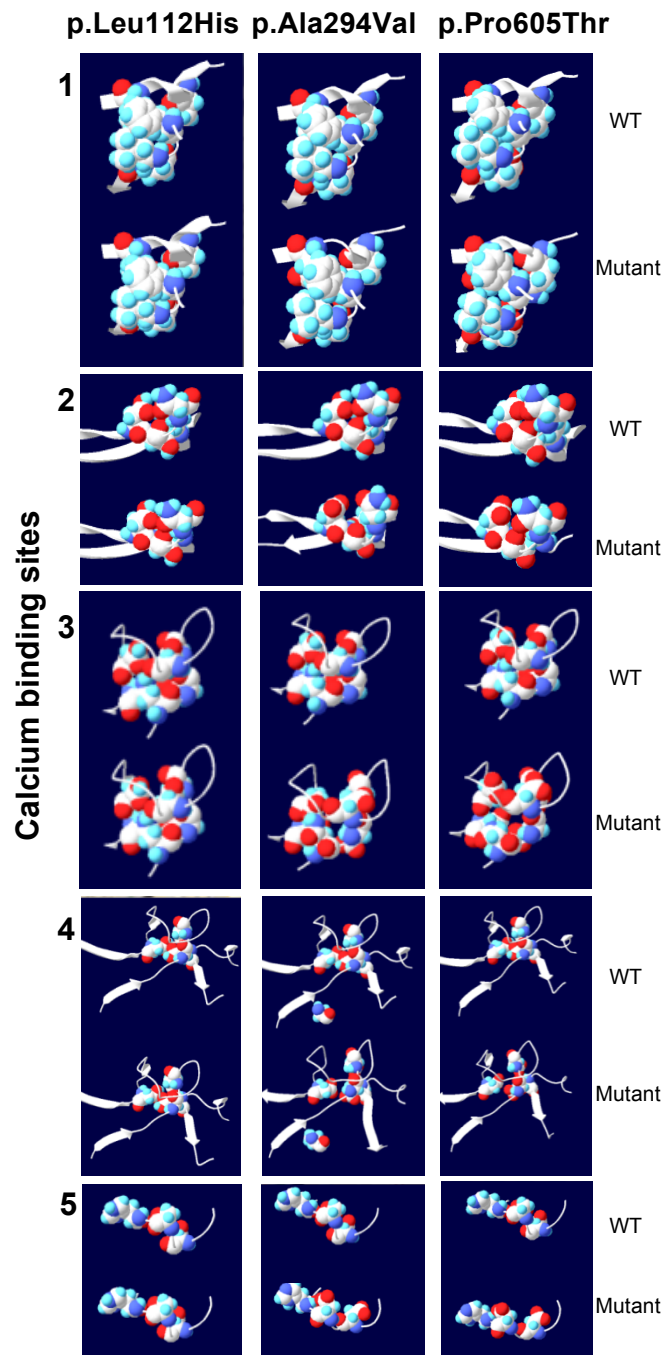


Figure S5

Topological tridimensional models of WT and mutant PADI3: Predicted calcium binding sites

Zoom on the amino acids involved in the five calcium-binding sites (1-5). As previously published,⁵ these amino acids (Table S2) were defined by analogy, after a multiple alignment, to the residues of the five calcium binding sites of PADI4 [MIM 605347].⁶ None of the substituted amino acids are directly involved in calcium binding. Nevertheless, the predicted models of p.Ala294Val and p.Pro605Thr mutants show clear spatial modifications of, at least, the calcium-binding sites 2-5.

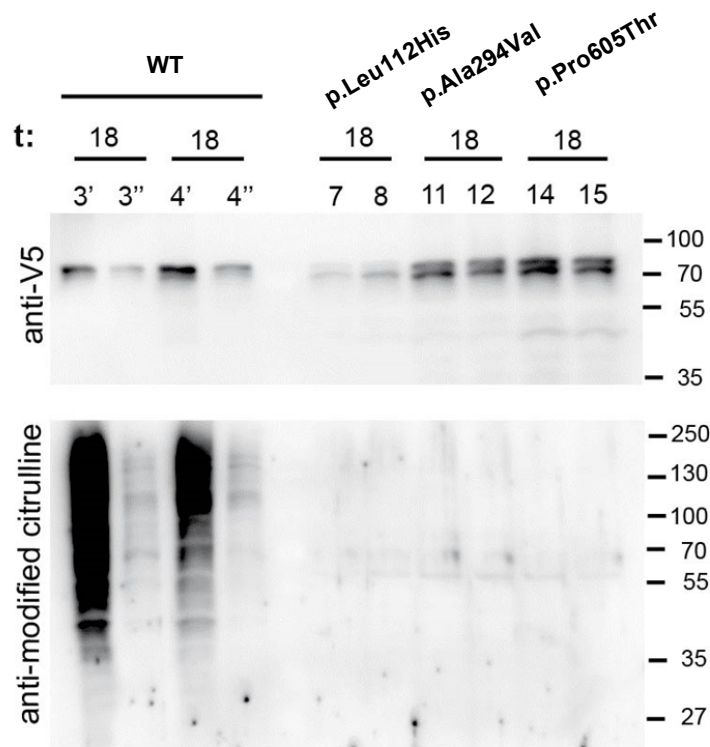


Figure S6

Absence of activity of mutant PADI3 produced in bacteria

Extracts of *E. coli* producing WT PADI3 were diluted either four (3' and 4') or eight times (3'' and 4'') in order to adjust the amounts of PADI3, as compared to undiluted extracts containing the mutant enzymes, p.Leu112His (clones 7 and 8), p.Ala294Val (clones 11 and 12) and p.Pro605Thr (clones 14 and 15). The extracts were then incubated for 18 hours with calcium, as indicated. After incubations, proteins were immunodetected with either the anti-V5 antibody or anti-modified citrulline antibodies. While citrullinated proteins were detected in the WT-containing extracts, no citrullinated proteins were detected in the mutant-containing extracts. Molecular mass markers are indicated on the right in kDa.

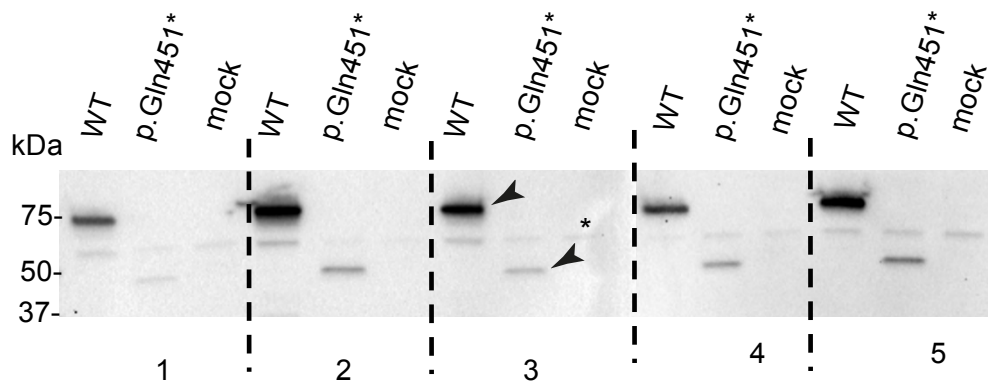
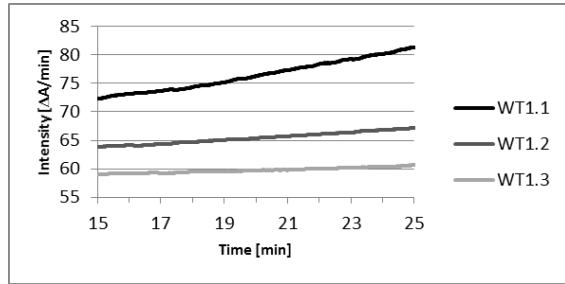


Figure S7

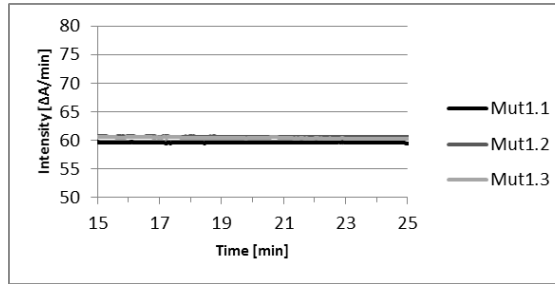
Immunoblotting of HEK293T extracts producing WT and mutant TGM3

Immunoblotting analysis shows the detection of WT and truncated TGM3 in transiently transfected HEK293T cells, which were collected 48 h post-transfection. Cell extracts from independent transfections (1-5), were concurrently immunoblotted (1-3, 4-5) with an anti-Flag antibody. Antibody-specific bands showing the WT (~70 kDa) and truncated TGM3 (~40 kDa) are indicated with an arrow and a non-specific cross-reactive band around 55 kDa is indicated with an asterisk. A persistent lower detection level was observed for the mutated protein in comparison to the WT TGM3. Relative protein quantification was performed using Stain-Free technology that is based on normalization by the total lane protein content (Bio-Rad Laboratories).

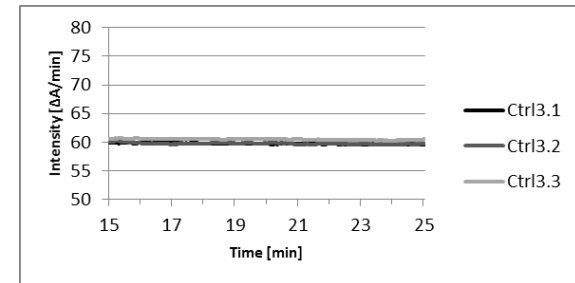
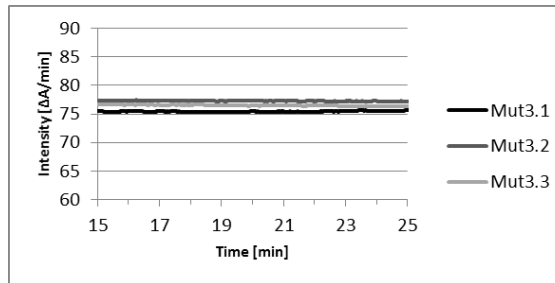
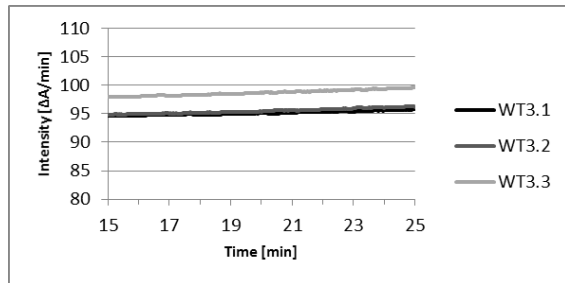
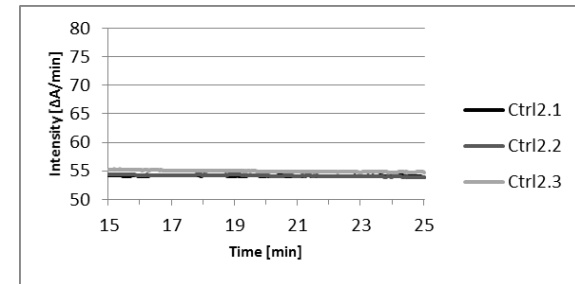
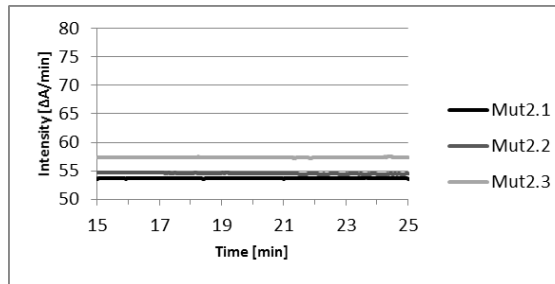
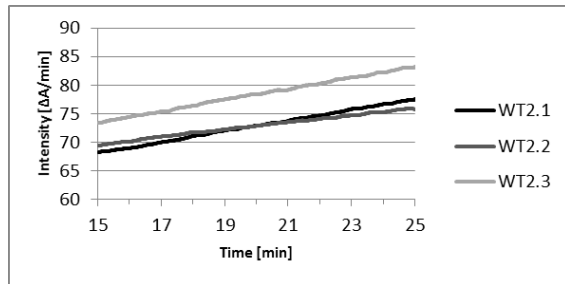
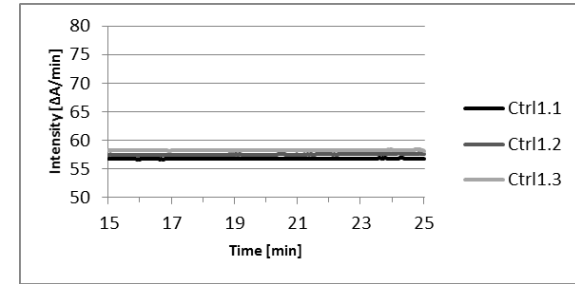
WT



Mut



Ctrl



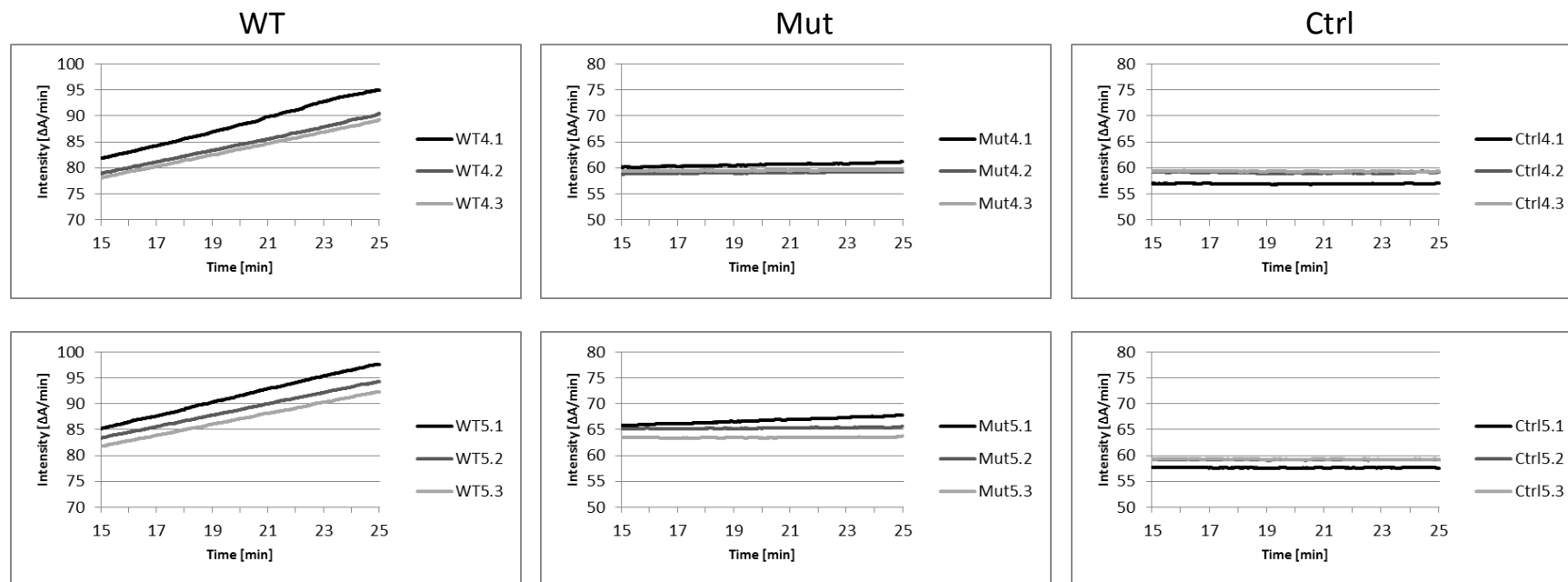


Figure S8

Transglutaminase activity of TGM3 produced in HEK293T cells

Fluorescence intensity augmentation by incorporation of monodansylcadaverine into casein. Measurements from five independent transfections are presented in rows. Three technical replicates for each sample are depicted with color-coded lines. Linear slopes of the measurements represent the transglutaminase activity.

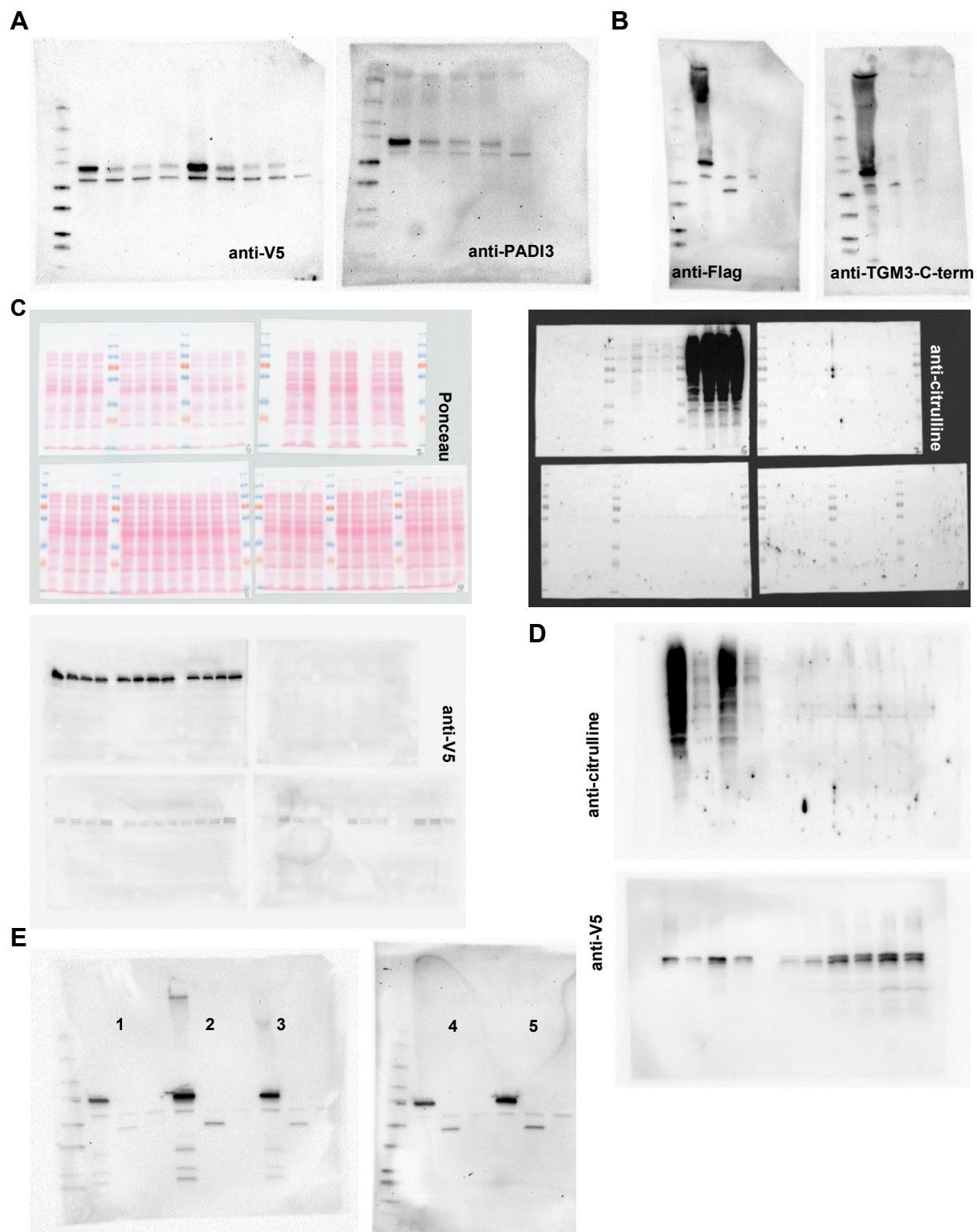


Figure S9

Full-length gel and blot images from the main figures.

Full-length images of the blots/gels in **(A)** Figure 4A, **(B)** Figure 7A, **(C)** Figure 5B, **(D)** Figure S6 and **(E)** Figure S7

Supplemental Tables

Table S1. Primers used for sequencing of *PADI3*

Amplicon	Forward (5'-3')	Reverse (5'-3')
PADI3_Ex1	CTGAGCTCTCAGCTCTGGGA	TCTTCTACCTGGCTCAGCC
PADI3_Ex 2	GCTTGACTCGCAGGAGCTTA	TCTGTAACCTGCAGAGCTGG
PADI3_Ex 3	GGCACAGAGGAGGTAAAGAA	TCCATTTGTGGAGGCTTAGC
PADI3_Ex 4	CCTCTTGATGGTGTCTCCTT	AGTCCAGAAGGTCTTGATCCC
PADI3_Ex 5	GCCATTGACATGTCTTGAGAA	AGCATCGAGGTGTGTCTGG
PADI3_Ex 6	CAGCTGGCTATGCCACACT	TTCTGACTGTTCTTACTGCG
PADI3_Ex 7	CCACTGTGTATTACCTGTCCT	TGATCATGGCTCACTGCAAC TAGGTTACACCCTATACC*
PADI3_Ex 8/9	GGTTCATTTCCATCTTGACAGA	TGTTGAATCCAGGATCAGC
PADI3_Ex 10	CTGACCTGGGCACATTTATG	TTTAGGGCTGCCAGATTCAG
PADI3_Ex 11	CTCAGGCTCCATGTCCGAT	AATGATCTCTTAGGTCTCTGC
PADI3_Ex 12/13	AGATTTTCCTGGATGGTGGG GCAGGAATGCTAAACTCTTGT*	AGTCCATGTCCACCTTCTATC
PADI3_Ex 14/15	GGCTGCTGACTCGGCAAGA	TCCCAGCTGATGCCATGTGC
PADI3_Ex 16	CCAGAGTGAGTTCTGCGGAT	AAGTCTGAGAACCACATGGG

Primer pairs are used both for amplicon generation and Sanger sequencing reactions. *Additional primers were used for the cycle sequencing reaction in order to cover the whole region.

Table S2. Primers used for sequencing of *TGM3*

Amplicon	Forward (5'-3')	Reverse (5'-3')
TGM3_Ex 1	AGGCAATCCTTGGCAGCCTG	GATGTCCAGCTGCACTGAACA AAGGCAGGCAGCTGTCTGG*
TGM3_Ex 2	AGGATGCACAGAGGTTCCAGC	AGAGATGGACAGCAACTTGC
TGM3_Ex 3	GTTGTATTGGAACCTGGTCT	TGCTTAAGTGTGTCAGAGCTCC TAGGCCAGGGCTGAGAGTGTG*
TGM3_Ex 4	AAGCAGCTGTCTGAGTGTGG	ACACTAAGGAAGTGTGCATCGC
TGM3_Ex 5	TCAGTAGCTCTCAGTTCCAG	TACTCACTGTGTGCCTCAGG
TGM3_Ex 6/7	ACTGTGACAGCAGTGATAGCC	AGACTAGCAGACCGCAGAGC GTGAGAGCGAGAAGCCACTCA*
TGM3_Ex 8	ACTCACTCGATGCATGTTGTC	AGGCTCTGTGCAGCAACAGTG
TGM3_Ex 9	TTGCAGTGGTCCTGGAAGGC	AGGCAGAACTGGCTGCCAGTG
TGM3_Ex 10	TCCGGTTAAGACAGGCGAGC	TGTGCCATAGCTATGAACTGC
TGM3_Ex 11	TGGCCAAGGAGGGCTCAGTC	TGGGAGAGCTGTGGCTCACAG
TGM3_Ex 12	AGCACAGGATAATGTCCTGG	AGATTCTAGAGTTCCAAGACC
TGM3_Ex 13	AACAGGACAGGAGGTCACAG	TCCATGGTGAGCTCTCCCTG

Primer pairs are used both for amplicon generation and Sanger sequencing reactions. *Additional primers were used for the cycle sequencing reaction in order to cover the whole region.

Table S3. Primers used for sequencing of *TCHH*

Primer Name	Sequence (5'-3')
TCHH_EX 2F	GGTGGAGAGCTGGAAGAAAGACA
TCHH_EX 2R	TGGGGGATGTAGTGTAGACCTGTT
TCHH_EX 3F	TGAGCTCTTCATGGGACATTACCACA
TCHH_EX 3R	TGCACTTTCCACAAGATGGGTCA
<i>TCHH_SF1</i>	<i>GCTCTGAATGTCTCTTGAATGTCA</i>
<i>TCHH_SF2</i>	<i>CAAAGGCAAGAATGGCAAGAA</i>
<i>TCHH_SF5</i>	<i>CTAGCTGAGGAGGAGCAGGAACA</i>
<i>TCHH_SF6</i>	<i>GTGGCAACTAGAAGAAGAAAGGA</i>
<i>TCHH_SF8</i>	<i>CAAAGGCAGAGAGAATGAACAGTT</i>
<i>TCHH_SF16</i>	<i>CAGCAGCGGGACAACGGTTTCT</i>
<i>TCHH_SF20</i>	<i>CGAACAGGAAGTGCAGTCAGGA</i>
<i>TCHH_SF23</i>	<i>GAGCAGCTGCTGAGAGAGGAACA</i>
<i>TCHH_SEQ1F</i>	<i>TGGAGCGCAAGAGCTGAG</i>
<i>TCHH_SEQ3F</i>	<i>TCGGAAGGATAAGAAGCTG</i>
<i>TCHH_SEQ5F</i>	<i>AGAGTCGTCGTGAGGAACAAG</i>
<i>TCHH_EX3.2F</i>	<i>CGCAGGCAGAAGAGGCAGGAA</i>
<i>TCHH_EX3.3F</i>	<i>GCGGTTGAGGAGCGAGCAAC</i>
<i>TCHH_EX3.4F</i>	<i>CCAGCAGCGGGAACAACGGT</i>
<i>TCHH_EX3.5F</i>	<i>GCGGGAGAGGCAGTATCGGG</i>
<i>TCHH_EX3.6F</i>	<i>CAGCGCGACAGGCATTTCC</i>
<i>TCHH_EX3.7F</i>	<i>CAACAGCTGCGTCACGACCG</i>
<i>TCHH_EX3.1R</i>	<i>CTGTCTTGCCGCTCTCGCCT</i>
<i>TCHH_EX3.3R</i>	<i>CTTGCGTACAGCGTGTGGC</i>
<i>TCHH_EX3.4R</i>	<i>TGTCGCGCAGCTGGGAATCT</i>
<i>TCHH_SR2</i>	<i>TCCTTTCTTCTTCTAGTTGCCAC</i>
<i>TCHH_SR3</i>	<i>CAGCTTCTTATCCTTCCGA</i>
<i>TCHH_SR4</i>	<i>AACTGTTCAATTCTCTCTGCCTTTG</i>
<i>TCHH_SR5</i>	<i>CTTGTTCTCACGACGACTCT</i>
<i>TCHH_SR9</i>	<i>GACGGAGCTGCTTCTCTTAGGAT</i>
<i>TCHH_SR10</i>	<i>CCAGCGATACTTTCCGTACGCTGTT</i>
<i>TCHH_SR11</i>	<i>GAGGAAGAACAGCTGGAGCGAGA</i>

Primer pairs used for amplicon generation are given in bold and primers used for cycle sequencing reactions are given in italic. Presence of *TCHH* mutations in the coding sequence in screened individuals could not be entirely excluded as overlapping and/or individual regions could not be sequenced in different individuals due to technical limitations arising from the repetitive regions.

Table S4. Primers used for cloning and mutagenesis

Construct	Primers
PADI3 WT	PADI3-WT-F: 5' accATGTCGCTGCAGAGAATCGTG 3' PADI3-WT-R: 5' GGGCACCATGTTCCACCAC 3'
PADI3 p.Leu112His	PADI3-Mut-p.L112H-F: 5' CCTATGCGGTGCTCTACC AC ACCTGTGTTGACATCTC 3' PADI3-Mut-p.L112H-R: 5' GAGATGTCAACACAGGTGTGGTAGAGCACCGCATAGG 3'
PADI3 p.Ala294Val	PADI3-Mut-p.A294V-F: 5' GTGGTGTTCGGAGTGGTACCCTGGATCATGACG 3' PADI3-Mut-p.A294V-R: 5' CGTCATGATCCAGGGT ACC ACTCGGAACACCAC 3'
PADI3 p.Pro605Thr	PADI3-Mut-p.P605T-F: 5' CCCC AAG CCCTTTGGG ACC ATCATCAATGGCTG 3' PADI3-Mut-p.P605T-R: 5' CAGCCATTGATGATGGTCCCAAAGGGCTTGGGG 3'
TGM3 WT	TGM3-WT-F: 5' accatg <i>gattacaaggatgacgacgataagccaggacca</i> ATGGCTGCTCTAGGAGTCC 3' TGM3-WT-R: 5' TCATTGGCTACATCGATG 3'
TGM3 p.Gln451*	TGM3-Mut-p.Q451*-F: 5' GCTCTGACCAGGAAAGATAAGTGTTC CAA AAGGCT 3' TGM3-Mut-p.Q451*-R: 5' AGCCTTTTGGAACTT AT CTTTCTGGTCAGAGC 3'

The N-terminal flag tag sequence fused to *TGM3* is given in italic. The locations of the mutations are given in bold in the respective mutagenesis primers. WT; wild type; Mut, mutant; F; forward; R; reverse

Table S5. *PADI3*, *TGM3* and *TCHH* mutations in ExAC database

Variant^a	Gene	Consequence	Allele count	Total allele	Homozygous individuals	Allele frequency
1:17588689 T / A (rs142129409)	<i>PADI3</i>	p.Leu112His	459	111360	0	0.004122
1:17597423 C / T (rs144080386)	<i>PADI3</i>	p.Ala294Val	809	121318	5	0.006668
1:17609392 C / A (rs144944758)	<i>PADI3</i>	p.Pro605Thr	51	113490	0	0.0004494
20:2312665 C / T (rs779702016)	<i>TGM3</i> *	p.Gln451*	1	114212	0	0.000008756
1:152084702 G / A (rs201930497)	<i>TCHH</i> *	p.Gln331*	43	112892	0	0.0003809

^aVariants are annotated by genomic location based on hg19, nucleotide substitution and their dbSNP IDs.* None of the sequenced individuals in ExAC database carry a loss of function mutation in homozygous state in these genes.

Table S6. Amino acid residues and positions[#] involved in the 5 calcium binding sites and the catalytic site of PADI3

Calcium binding sites	Residue-position
1	Gln-349 / Glu-353 / Phe-407 / Leu-410 / Glu-411
2	Glu-351 / Asp-369 / Ser-370 / Asn-373
3	Asn-153 / Asp-155 / Asp-157 / Asp-165 / Asp-176 / Asp-179
4	Asp-155 / Asp-157 / Asp-179 / Asp-388
5	Asp-165 / Asp-168 / His-170
Catalytic site*	Asp-350 / His-470 / Asp-472 / Cys-646

[#]Positions of calcium-coordinating and catalytic site residues are reported according to the PADI3 primary sequence (GenBank accession number AB026831) after a multiple alignment, as previously described.⁷ They have been defined by analogy to the analysis of PADI4 crystal structure analysis.⁶ *The 4 major amino acids of the catalytic site are mentioned.

Supplemental References

1. Nissen, C.V., and Svendsen, M.T. (2013). [Uncombable hair syndrome]. *Ugeskr Laeger* 175, 2878.
2. Novoa, A., Azon, A., and Grimalt, R. (2012). [Uncombable hair syndrome]. *An Pediatr* 77, 139-140.
3. Kilic, A., Oguz, D., Can, A., Akil, H., and Gurbuz Koz, O. (2013). A case of uncombable hair syndrome: light microscopy, trichoscopy and scanning electron microscopy. *Acta Dermatovenerol Croat* 21, 209-211.
4. Corpet, F. (1988). Multiple sequence alignment with hierarchical clustering. *Nucleic Acids Res* 16, 10881-10890.
5. Mechin, M.C., Coudane, F., Adoue, V., Arnaud, J., Duplan, H., Charveron, M., Schmitt, A.M., Takahara, H., Serre, G., and Simon, M. (2010). Deimination is regulated at multiple levels including auto-deimination of peptidylarginine deiminases. *Cell Mol Life Sci* 67, 1491-1503.
6. Arita, K., Hashimoto, H., Shimizu, T., Nakashima, K., Yamada, M., and Sato, M. (2004). Structural basis for Ca(2+)-induced activation of human PAD4. *Nat Struct Mol Biol* 11, 777-783.
7. Mechin, M.C., Sebbag, M., Arnaud, J., Nachat, R., Foulquier, C., Adoue, V., Coudane, F., Duplan, H., Schmitt, A.M., Chavanas, S., et al. (2007). Update on peptidylarginine deiminases and deimination in skin physiology and severe human diseases. *Int J Cosmet Sci* 29, 147-168.